AD-A064 726 AIR FORCE INST OF TECH WRIGHT-PATTERSON AFB OHIO SCH--ETC F/G 17/1
SIMULTANEOUS NON-HOMOGENEOUS MULTIPLE ACCESS TECHNIQUES.(U)
DEC 78 P RODRIGUEZ

UNCLASSIFIED AFIT/GE/EE/78-39 NL

1 OF
AD
AD 64726

END
DATE
FILMED
4-79
DDC

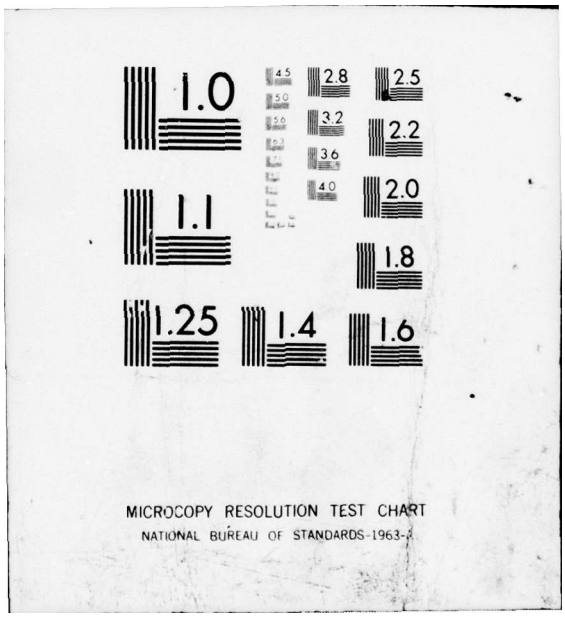
1.0
1.1
1.25
1.4
1.6
1.8
2.0
2.2
2.5
2.8
3.2
3.6
4.0
4.5
5.0
5.6
6.3
MICROCOPY RESOLUTION TEST CHART
NATIONAL BUREAU OF STANDARDS-1963-A

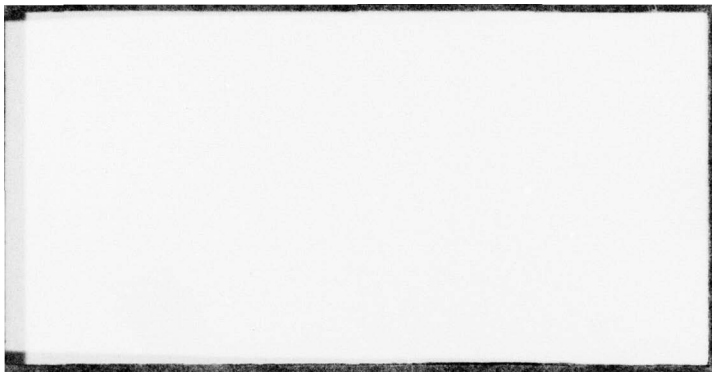

AFIT/GE/EE/78-39

(1)

AD A064726

DDC FILE COPY

# SIMULTANEOUS NON-HOMOGENEOUS MULTIPLE ACCESS TECHNIQUES

THESIS

AFIT/GE/EE/78-39 Pedro Rodriguez
Capt. USAF



Approved for public release; distribution unlimited.

JOSEPH P. HIPPS, Major, USAF
Director of Information

19 Jan 79

see title page

(17)
AFIT/GE/EE/78-39

(6) SIMULTANEOUS NON-HOMOGENEOUS MULTIPLE ACCESS TECHNIQUES.

(9) Master's THESIS,

Presented to the Faculty of the School of Engineering
of the Air Force Institute of Technology
Air Training Command
in Partial Fulfillment of the
Requirements for the Degree of
Master of Science

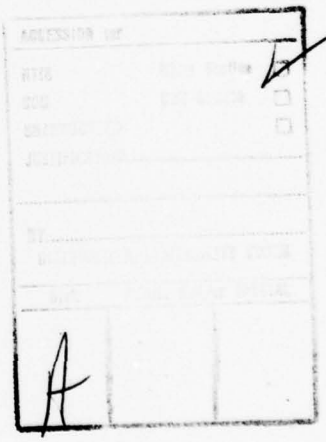

by

(10) Pedro Rodriguez, B.S.
Capt. USAF
Graduate Electrical Engineering

(11) December 1978

(12) 86 p.

Approved for public release; distribution unlimited.



012225 B

## Preface

The purpose of this thesis was twofold. The first was to satisfy the School of Engineering thesis requirement. The second was to investigate a satellite transponder system which is already in the development stage to determine the best use of that system when accessed by the equipment presently in use and planned to become operational in the near future. A study of a communications control system was originally part of the topic. Control systems are presently being investigated feverishly. Most articles which have been published recently conclude that the control function should be placed at the satellite.

I am extremely grateful to Capt. Thourot from Hq. AFCS, who submitted a proposal for consideration as a thesis topic from which this thesis topic was extracted. I wish to thank my readers, Maj. Cappinella and Capt. Hadley. I wish to express appreciation to Asst. Prof. Joseph Carl of the Department of Electrical Engineering, for his helpful guidance, and counseling during this study. I owe a special thank you to Mrs. Weber, who typed the final copy.

I wish to express fatherly love to my daughters who often experienced my wrath brought about by school stresses, and brought about, they must have felt, for no apparent reason. I wish to thank my wife for her patience and consideration without which this work would never have been completed. I dedicate this effort to my soon-to-be-born child.

Pedro Rodriguez

## Contents

## List of Figures

## List of Tables

## List of Symbols

| | |
|---|---|
| BPL | Bandpass Limiter |
| BPSK | Binary Phase Shift Keyed |
| BW | Bandwidth |
| $E_b$ | Signal-Energy-per-Bit |
| FDMA | Frequency Division Multiple Access |
| $H_0$ | Hypothesis that signal $s_0$-plus-noise is present |
| $H_1$ | Hypothesis that signal $s_1$-plus-noise is present |
| $I_0$ | Modified Bessel Function of the first kind order zero |
| $I_1$ | Modified Bessel Function of the first kind order one |
| IM | Intermodulation |
| IMP's | Intermodulation products |
| $J_0$ | Bessel Function of the first kind order zero |
| $J_1$ | Bessel Function of the first kind order one |
| $N_o$ | Noise Density |
| $P_e$ | Probability of Error |
| QPSK | Quadriphase Phase Shift Keyed |
| pdf | Probability Density Function |
| r-f | Radio Frequency |
| SNR | Signal-to-noise ratio |
| TDMA | Time Division Multiple Access |
| TWT | Traveling-wave-tube |

## Abstract

The possibility of using simultaneous non-homogeneous multiple access techniques through a common transponder channel was investigated. Three configurations were analyzed: (1) a single time division multiple access, (2) several frequency division multiple accesses, and (3) the combined accesses of configurations (1) and (2). Each of the configurations was studied in three disjoint segments: (1) the bandwidth and shape of the power spectrum for various modulating waveforms, (2) the probability for error for linear PSK and non-linear PSK systems, and (3) the distortion effects that a signal experiences through a non-linearity. Each segment was studied in detail independently of the others. The comprehensive analysis accomplished on each segment, when joined into a system, allows the end-to-end channel characterization. A link calculation was accomplished for a single TDMA access, because it was found to be the optimum system based on the analysis of the segments. Also, the results obtained indicate that the benefits derived by using non-homogeneous accesses through a common transponder channel are far less than the total degradation the system experiences. A recommended alternative is provided.

# SIMULTANEOUS NON-HOMOGENEOUS MULTIPLE ACCESS TECHNIQUES

## I. Introduction

### Background

The Defense Satellite Communications System (DSCS) Program currently includes research and development of and plans to phase-in time division multiple access (TDMA) equipment. It is anticipated by Headquarters Air Force Communications Service (AFCS) that during the middle 1980's a transition will occur in the use of satellite multiple access techniques from frequency devision multiple access (FDMA) to TDMA. The use of FDMA will not immediately cease when this transition takes place, but will continue for the duration of the FDMA equipment's useful life. It is for that reason that this study was accomplished to determine possible problems which might be encountered when both multiple access techniques are used simultaneously through the same satellite transponder.

### Problem

The problem that was addressed was one of intermodulation products and signal suppression factors. For TDMA, a transponder is operated at saturation to take full advantage of the traveling-wave-tube (TWT) output power. For FDMA, since several carrier frequencies are present at the transponder input, the power level of each carrier must be monitored and

controlled to minimize intermodulation; nevertheless, intermodulation products still result and reduce the available output power of the desired signals. When FDMA and TDMA are used simultaneously through the same transponder, the weaknesses inherent in each are present. The purposes of this study are to investigate those weaknesses to find an alternative or alternatives that make the best use of the transponder's available power and bandwidth, and to provide recommendations as to the best alternative.

## Scope

This study dealt almost entirely with the analysis of a transponder accessed simultaneously by FDMA and TDMA techniques to determine what degradations, if any, occur in the system. Theoretical concepts that are closely related to the problem under study are included in this report. This study does not address the communications control or synchronization timing problems, since those problems will be solved during the design of the TDMA equipment subsequent to this study. The DSCS III space segment and the SHF Ground Mobile Forces (GMF) terminals are included as constraints on the analysis, but in reality, the analysis is equally applicable to other similar systems.

## Assumptions

Three assumptions were made and are stated as follows: the noise which corrupts the transmission channel is white Gaussian noise which has zero mean and has a flat power spectrum, the noise bandwidth is much smaller than the center

frequency of the bandpass filter, and the bandpass filter which precedes and the zonal bandpass filter which follows the limiter are wide enough to pass the desired signal with negligible distortion.

## Summary of Current Knowledge

Of the three generic satellite multiple access techniques, TDMA, FDMA, and spread-spectrum multiple access (SSMA), TDMA achieves the best power and bandwidth efficiency. The power efficiency advantage of TDMA results from the lack of intermodulation distortion, since only one carrier is present at the transponder. Overhead bits which are required for guard time, synchronization, and network control functions reduce the power efficiency. In FDMA, power losses result from intermodulation, which is created by multiple accesses occupying the transponder simultaneously, and suppression of one signal by another. To reduce intermodulation the transponder is backed-off from saturation to a nearly linear operating region, but this results in power efficiency loss and capacity loss due to reduced down link effective radiated power (ERP). Another FDMA loss occurs in the use of real filters which have non-ideal roll-off characteristics, so that a guard band has to be provided between accesses to keep the losses due to cross-talk to a tolerable level.

## Approach

The problem was analyzed in three configurations which are as follows: 1) a single TDMA carrier and its optimum

performance, 2) several FDMA carriers and their optimum performance, and 3) a compromise configuration consisting of a single TDMA signal and several FDMA signals. The performance parameters were found for each of the three cases listed above. However, before the performance parameters could be determined it was necessary to segment the problem into disjoint parts and to analyze those parts in detail.

The individual parts of the problem as finally segmented follow: 1) the derivation of the power spectrum for phase-shift-keyed modulation, 2) the analysis of a bandpass limiter when it is in a hard and soft configuration, and 3) the detection of the PSK signal through linear and non-linear limiters. Once the individual parts were analyzed, the pieces were joined and studied as a whole. Link calculations were then possible since the parameters for each segment were known. In addition, the several cases of concern were analyzed to determine the feasibility of using simultaneous non-homogeneous multiple access techniques through a common transponder channel.

A large amount of information is available on this subject. Many of the figures included herein were generated from equations found in the literature and were numerically evaluated by the computer. The results obtained were then plotted by the calcomp plotter. Most of the equations found in the literature involved Bessel functions, so graphical results are provided as visual aids to make clear the significance of those equations.

## II. Power Spectrum

The power spectrum of digital angle modulated signals can be calculated in many ways. The direct way of calculating the power spectrum is to first find the Fourier transform of a sample of the signal on a finite interval. This approach was used here. However, the double Fourier transform had to be used since the signal under consideration was found to be non-stationary.

Digital binary phase-modulated signals can be represented as

$$x(t) = \sum_{n=0}^{N} b_n \cos(w_c t) p(t-nT) \qquad (1)$$

where the $b_n$'s are identically independently distributed random variables which each take values +1 and -1 with equal probability, and p(t) is the binary pulse. In this analysis p(t) is a rectangular pulse of time duration T.

### Derivation

The power spectral density of the random process is the Fourier transform of the autocorrelation function which is obtained from

$$R_x(t_1, t_2) \leftrightarrow S_x(f) \qquad (2)$$

where

$$R_x(t_1, t_2) = R_x(t_1 - t_2) \qquad (3)$$

Also, autocorrelation is equal to the expected value of the random process sampled at two arbitrary time instances. It is expressed as

$$R_x(t_1,t_2) = E[x(t_1)x(t_2)]$$

$$R_x(t_1,t_2) = E\left\{ \sum_{n=0}^{N} b_n \cos w_c t_1 \; p(t_1-nT) \right.$$

$$\left. \cdot \sum_{m=0}^{N} b_m \cos w_c t_2 \; p(t_2-mT) \right\}$$

$$= \cos w_c t_1 \cos w_c t_2 \sum_{n=0}^{N} \sum_{m=0}^{N} E\, b_n b_m \cdot p(t_1-nT)p(t_2-mT) \quad (4)$$

But

$$E[b_n b_m] = \begin{cases} 0, & m \neq n \\ 1, & m = n \end{cases} = \delta_{mn}, \text{ the Kronecker delta, so}$$

$$R_x(t_1,t_2) = \cos w_c t_1 \cos w_c t_2 \sum_{n=0}^{N} p(t_1-nT) \cdot p(t_2-nT) \quad (5)$$

Now, since $p(t_1-nT)$ and $p(t_2-nT)$ are both sample values of the same shifted rectangular pulse (which is non-zero only on an interval of length T), their product is non-zero only if $t_1$ and $t_2$ lie in the same signaling interval of length T for exactly one value of n. In that case, and that case only, the product has the same value as the square of the pulse amplitude, say $A^2$; otherwise the product is zero. Thus,

$$R_x(t_1,t_2) = \begin{cases} A^2 \cos w_c t_1 \cos w_c t_2, \text{ if } t_1 \text{ and } t_2 \text{ lie in the same signalling interval} \\ 0, \text{ else} \end{cases}$$

A process is stationary in the wide sense if its expected value is a constant and its autocorrelation depends only on the difference $\tau = t_1 - t_2$. The process in Eq (5) has values other than zero when the selected arbitrary time instances fall in the same signaling interval and is identically zero when the selected arbitrary time instances fall in different signaling intervals. Since the cosine terms are also expressible as

$$\cos w_c t_1 \cos w_c t_2 = \frac{1}{2}[\cos w_c(t_1+t_2) + \cos w_c(t_1-t_2)] \quad (6)$$

It is obvious that the random process under consideration does not have an autocorrelation function which is solely a function of $t_1 - t_2$. Hence, the process is not stationary, even in the wide sense. Its spectrum cannot be obtained from the Fourier transform of the autocorrelation function.

Because the autocorrelation functions of non-stationary processes are functions of two variables, in order to apply transform techniques, two-dimensional Fourier transforms are needed. The double Fourier transform, $\Gamma(w_1,w_2)$, of $R_x(t_1,t_2)$ can also be defined. The double Fourier transform can be represented as (Ref 12:466)

$$\Gamma(w_1,w_2) = E[X(w_1)X^*(w_2)] \quad (7a)$$

$$= \int_{-\infty}^{+\infty}\int_{-\infty}^{+\infty} R_x(t_1,t_2)e^{-j(w_1t_1-w_2t_2)}dt_1dt_2 \quad (7b)$$

Thus, since the process at hand is non-stationary, this more general approach for finding the power spectrum must be used.

The random process will be first transformed into the frequency domain using the Fourier transform. The expected value of the new random process multiplied by its conjugate yields the expression that represents the power spectrum of the random process. The random process in the frequency domain is given by

$$X(f) = \sum_{n=0}^{N} b_n \frac{1}{2}\{\delta(f-f_c) + \delta(f+f_c)\} * [P(f)\cdot e^{j2\pi fnT}] \quad (8a)$$

$$X(f) = \sum_{n=0}^{N} b_n \frac{1}{2}[P(f-f_c) + P(f+f_c)]e^{j2\pi fnT} \quad (8b)$$

and its conjugate

$$X(f) = \sum_{m=0}^{N} b_m \frac{1}{2}[P^*(f-f_c) + P^*(f+f_c)]e^{-j2\pi fmT} \quad (8c)$$

Multiplying X(f) by X*(f), taking the expected value of the product, and assuming positive and negative frequency terms do not overlap yields

$$E[X(f)X^*(f)] = \frac{1}{4} \sum_{n=0}^{N} \sum_{m=0}^{N} [|P(f-f_c)|^2 + |P(f+f_c)|^2] \cdot E[b_n b_m]\cdot e^{j2\pi fT(n-m)} \quad (9)$$

But $E[b_n b_m] = \delta_{mn}$, so that if the cross-product terms like $P(f-f_c)P^*(f+f_c)$--it can be argued that $f_c$ is large enough that positive and negative frequency terms do not overlap--, then

$$E[X(f)X^*(f)] = \frac{1}{4}[\sum_{n=0}^{N} |P(f-f_c)|^2 + |P(f+f_c)|^2] \quad (10a)$$

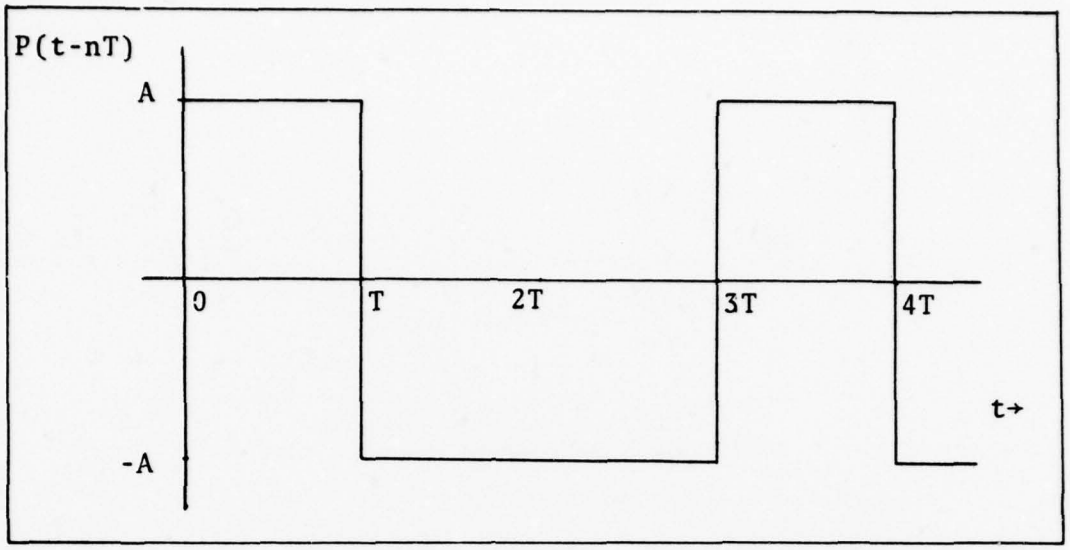


Fig 1. Typical Rectangular Modulating Waveform

or

$$E[|X(f)|^2] = \frac{N}{4}[|P(f-f_c)|^2 + |P(f+f_c)|^2] \qquad (10b)$$

The assumed form of the modulating signal is shown in Fig 1. The transform of a rectangular pulse is easily obtained from a transform-pair table. Most often the rectangular pulse is found shifted T/2 to the left in the transform table. However, since the only term sought here is the magnitude, the $e^{j\phi}$ and $e^{-j\phi}$ terms will cancel each other. The magnitude of the Fourier transform of p(t) can be found from

$$p(t-\tfrac{T}{2}) \leftrightarrow \hat{P}(f) = \frac{AT}{\pi fT} \sin \pi fT \triangleq AT \operatorname{sinc}(fT) \qquad (11)$$

$$|P(f)|^2 = |\hat{P}(f)|^2 = A^2T^2\operatorname{sinc}^2(fT) \qquad (12)$$

hence,

$$E[X(f)X^*(f)] = NA^2T^2/4\ [\operatorname{sinc}^2T(f-f_c)+\operatorname{sinc}^2T(f+f_c)] \qquad (13)$$

Comparison of Spectrum

The power spectrum, as derived and given by Eq (13), can be related to the results that Glance (Ref 5:2869) derived for a rectangular pulse of duration $\tau<T$. His results are given below. The continuous part of the spectrum is of the form

$$G(f) = (T/4)(\tau/T)^2 \{\sin[2\pi(f_c-f)(\tau/2)]/(f_c-f)(\pi\tau)\}^2 \quad (14)$$

but here $\tau=T$. With minor mathematical manipulations, Eq (14) can be written as

$$G(f) = (T/4) \{\sin[2\pi(f_c-f)(T/2)]/(f_c-f)(\pi T)\}^2 \quad (15)$$

which is identical to Eq (13).

Having pointed out that the results derived here for BPSK modulation agree with those of Glance, the results found in Glance's article are used hereafter since they are in a more general form. The trapezoidal waveform was used since it better represents a real baseband modulating signal. Now the modulating waveform appears as in Fig 2. It is composed of several signals that have been time division multiplexed into a continuous baseband data stream.

Binary Phase-Shift Keyed

Glance (Ref 5:2870-2871) has calculated the power spectrum for antipodal PSK modulation by a trapezoidal waveform. The spectrum has a continuous part and a discrete part as follows:

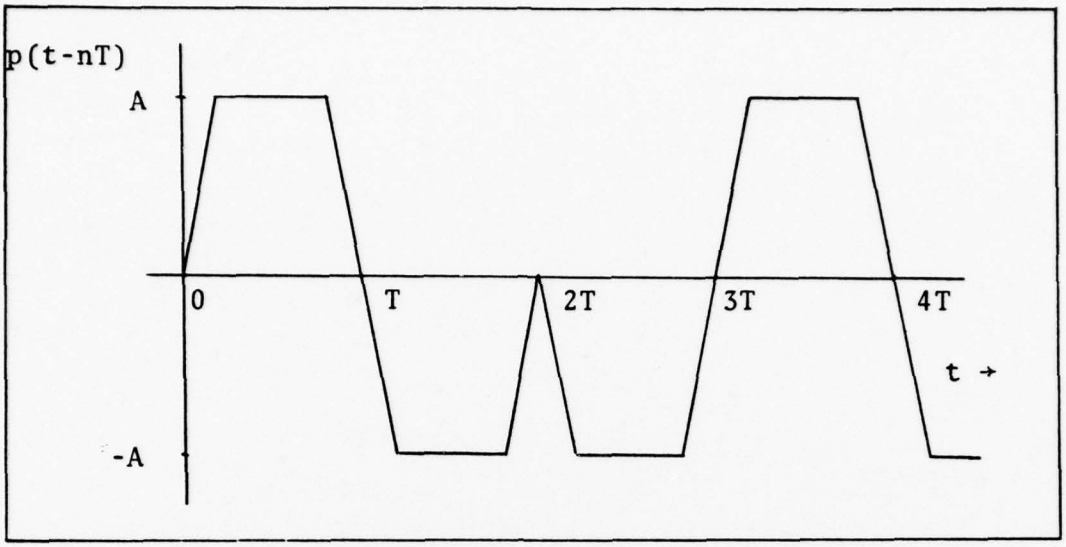


Fig 2. Baseband Modulating Signal Bit Stream

$$G_c(f) = \frac{T}{4}\left(\frac{\pi^2}{4}\right)\left\{\frac{\frac{\tau/T\ \sin[(f_c-f)(\pi\tau)]}{(f_c-f)\pi\tau} + \frac{S}{T}\cos[(f_c-f)(\pi T)]}{[(f_c-f)(S/2)]^2 - (\pi/4)^2}\right\}^2 \qquad (16)$$

for the continuous part, and

$$G_d(f) = \frac{1}{4}\left(\frac{\pi}{4}\right)^2\left(\frac{S}{T}\right)^2 \sum_{m=-\infty}^{\infty} \frac{\cos^2(2\pi m\ S/T)}{[(\pi m\frac{S}{T})^2 - (\pi/4)^2]^2}\ \delta(f_c+f+\frac{m}{T}) \qquad (17)$$

for the discrete part. Because this representation makes x(t) have zero mean, there is no discrete part to its spectrum. The power spectrum given by Eq (16) decreases as $1/f^4$ as $f\to\infty$. The spectral density and modulating signal representation for the continuous part are shown in Fig 3. The power spectra has a lower amplitude and greater bandwidth as the modulating rate is increased. This will become a very important relationship later when the power in the carrier is related to the

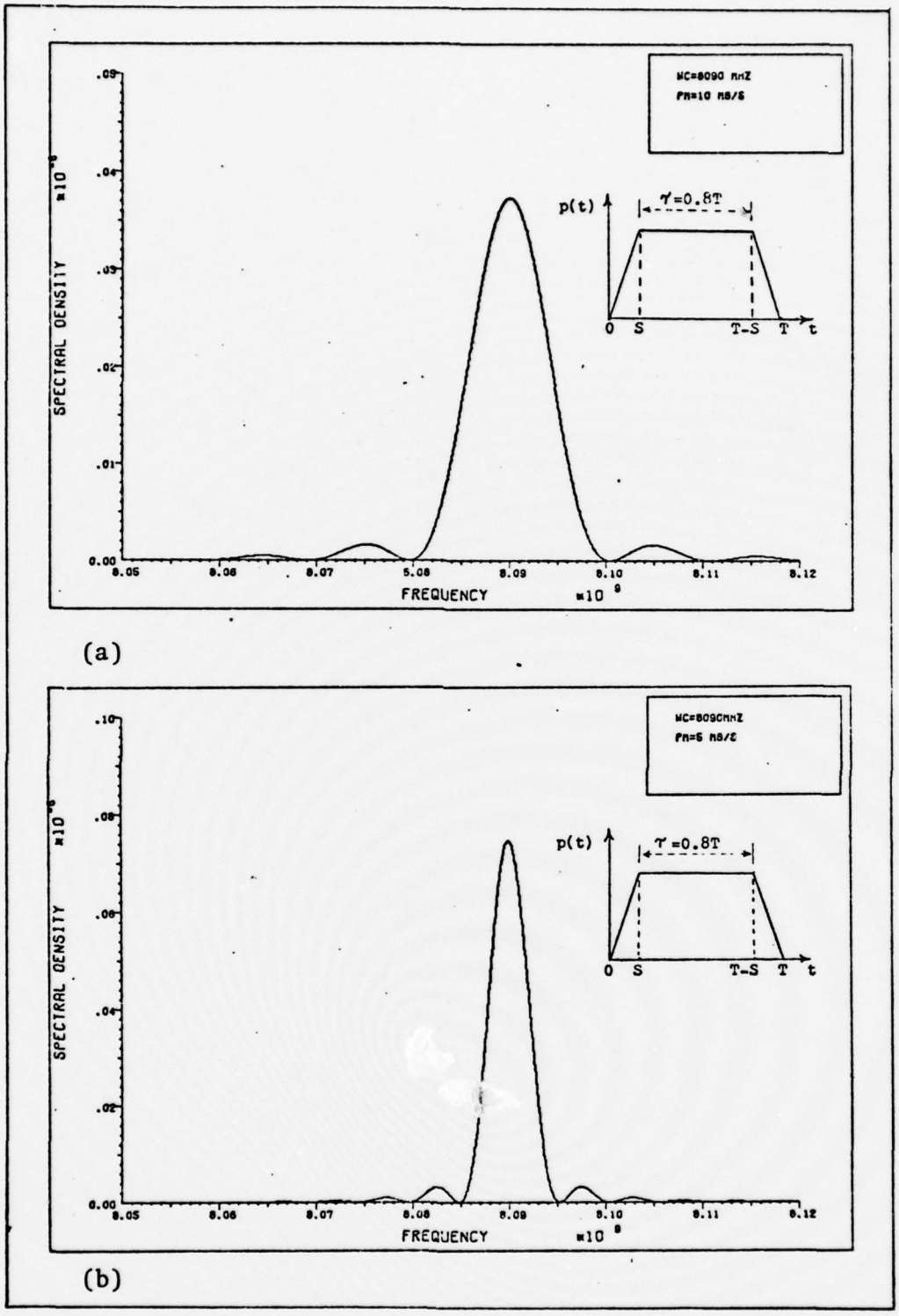


Fig 3. Spectral Density vs Frequency, (a) Phase Modulation - 10 Mb/s (b) Phase Modulation- 5 Mb/s

energy-per-bit-$E_b$. The energy-per-bit is defined as

$$E_b = A^2T/2 \tag{18}$$

where A is the amplitude of the sinusoidal constant envelope r-f carrier and T is the information bit time duration. For a BPSK signal with phase modulation rate of 10 Mb/s, the required bandwidth is 20 MHz. The bandwidth requirement is linearly related to the modulation rate. For BPSK, the bandwidth requirement is twice the modulation rate. For QPSK, the bandwidth is related to the modulation rate on a one to one basis.

## III. Bandpass Limiter

There are two effects that a signal passed through a limiter, such as a TWT, experiences. These effects are signal suppression and distortion. For instance, the results of this chapter show that the suppression a signal experiences in the presence of n signals which have equal magnitude is -1.05 dB. Additionally, their interaction in the non-linear device creates intermodulation products (IMP's) which further degrade the desired signal terms. How much signal suppression and distortion a non-linearity introduces into a communications channel is investigated in this chapter.

Moreover, a method is presented to reduce the harmful effects introduced by the non-linearity. Also, a method is presented to control the harmful effects of IMP's. These methods have been used extensively in the past. They use both the careful control of the drive levels to the input of the TWT and judicious frequency assignment of the r-f carriers.

### Hard-Limiter Suppression

An analysis of the output signal from the bandpass limiter shows the relationship between the input and output signal-to-noise ratio. The input-output relationship is determined for coherent and incoherent demodulation. The results obtained for each of the two cases are compared.

Communications Path Model. Figure 4 is a block diagram showing the bandpass limiter. In that figure, $h_1$ is a bandpass filter which has center frequency $w_c$, while $h_2$ is a zonal filter which selects the first zone components only. It is assumed that the bandwidth of the filter $h_1$ is much less than its center frequency.

The PSK signal plus noise is defined to be of the form

$$x(t) = s(t) + n(t) \tag{19}$$

where

$$s(t) = A \cos [w_c t + \phi(t)] \tag{20}$$

where $\phi(t)$ is a random phase process which takes values of 0 and $\pi$, and is the information bearing signal. The relationship to the notation in Chapter II should be clear. The noise is assumed to be white Gaussian noise expressed as

$$n(t) = n_c(t) \cos[w_c t+\phi(t)] - n_s(t) \sin[w_c t+\phi(t)] \tag{21}$$

where

$$E[n_s(t)] = E[n_c(t)] = 0 \tag{22}$$

$$E[n_s^2(t)] = E[n_c^2(t)] = \sigma_{n/2}^2 \tag{23}$$

and

$$\sigma_n^2 = N_o B_i \tag{24}$$

$B_i$ is the input bandwidth of filter $h_1$ in Fig 4. The ideal limiter function is defined as

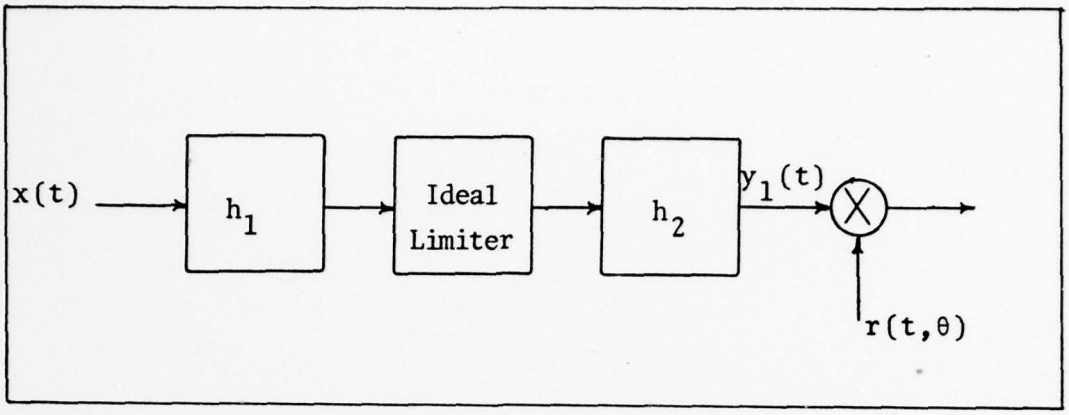


Fig 4. PSK System Block Diagram Model

$$y_L(t) = \text{sgn}\,[x(t)] = \begin{cases} +1, & x(t) > 0 \\ -1, & x(t) < 0 \end{cases} \tag{25}$$

Since

$$E[x(t)] = A\,E\{\cos[w_c t+\phi(t)]\} \tag{26}$$

the envelope of $y_L(t) = A$. Using trigonometric identities, the input process $x(t)$ can be written equivalently as

$$x(t) = a(t)\cos[w_c t+\phi(t)+\gamma(t)] \tag{27}$$

where

$$a(t) = \{[A+n_c(t)]^2 + n_s^2(t)\}^{1/2} \tag{28}$$

and

$$\gamma(t) = \tan^{-1}\{n_s(t)/[A+n_c(t)]\} \tag{29}$$

The signal given by Eq (27) has been analyzed by several individuals. Middleton (Ref 11:144) established the input-output time function relationship for the limiter using the complex Fourier transform. The output from the limiter as

derived by Middleton is given by

$$y_L(t) = 1/2\pi \int_c f(j\xi) \exp [j\xi x(t)] \, d\xi \qquad (30a)$$

where $f(j\xi) = 2/j$ is the Fourier transform of the dynamic path represented by the limiter. By expanding the exponential function in a series, the limiter output can be written as (Ref 16:43)

$$y_L(t) = 4/\pi \{\cos[w_c t+\gamma(t)+\phi(t)] + 1/3 \cos[3w_c t+3\gamma(t)+3\phi(t)]+ \ldots\} \qquad (30b)$$

The output of the limiter is represented by Eq (30b) as a series of phase-modulated sinusoids. This series begins with frequency $w_c$ and extends to all odd multiples of $w_c$. Since $h_2$ is a zonal filter which selects the first zone components only, the first zone output is

$$y_1(t) \triangleq 4/\pi \cos[w_c t+\gamma(t)+\phi(t)] \qquad (31)$$

In reality, a physical bandpass filter can only approximate the required output. However, because of the narrowband restriction which was stated earlier in this section, the error is small. The expected value of the power in the first zone components is (Ref 16:43)

$$E\{y_1(t)^2\} = 8/\pi^2 \qquad (32)$$

Incoherent Detection. The system under consideration is assumed to be coherent. However, the incoherent results are

included here for completeness. These results might prove useful later on or will serve to illustrate a point when compared to the coherent results.

Using Davenport's method (Ref 3) which amount to evaluating the amount of carrier component through formation of the second moment function and averaging over the distributions of $\phi(t)$ and $n(t)$, Springett and Simon (Ref 16) derive the bandpass limiter (BPL) input-output relationship. Their results follow in the remainder of this section. The first zone output is

$$y_1(t) = u(\rho) \cos[w_c t+\phi(t)+n'(t)] \tag{33}$$

where $n'(t)$ consists of the interaction of signal and noise (sxn), and noise and noise (nxn), and $u(\rho)$ is defined below. The limiter input SNR is $\rho$, defined as

$$(S/N)_i \triangleq \rho = A^2/2N_oB_i \tag{34}$$

The carrier component is now represented as a function of $\rho$ by

$$u(\rho) = (2\rho/\pi)^{1/2} e^{-\rho^2} \{I_o(\rho/2)+I_1(\rho/2)\} \tag{35}$$

where $I_o$ and $I_1$ are the modified Bessel functions of the first kind of order zero and one, respectively. The noise and signal power are now given as functions of $u(\rho)$, which is a function of $\alpha(\rho)$. The function $\alpha(\rho)$ is commonly referred to as the signal component suppression factor. The output noise power is given by

$$P_n = 8/\pi^2 - u(\rho)^2 = 8/\pi^2[1-\alpha(\rho)^2] \tag{36}$$

and signal power is given by

$$P_s = u(\rho)^2 = 8/\pi^2\ \alpha(\rho)^2 \tag{37}$$

which give an output SNR as

$$(S/N)_0^I = \frac{\alpha(\rho)^2}{[1-\alpha(\rho)^2]} \tag{38}$$

The superscript I denotes "incoherent," and the subscript 0 denotes "output."

Coherent Detection. The reference signal used for coherent detection is assumed to be of the form

$$r(t,\theta) = 2\ \cos[w_c t+\theta(t)+\phi(t)] \tag{39}$$

where $\theta$ takes values between $(\pi/2\ ,\ -\pi/2)$ and is the demodulation reference angle. The phase angle $\phi(t)$ is taken as known a priori. The signal and noise are as previously defined in Eqs (20) and (21) from which the output $y_1(t)$ of a BPL is derived as

$$y_1(t) = 4/\pi\ \cos[w_c t+\gamma'(t)] \tag{40}$$

where

$$\gamma'(t) = \tan^{-1}\{\frac{A\ \sin\ \phi(t)+n_s(t)}{A\ \cos\ \phi(t)+n_c(t)}\} \tag{41}$$

After substituting the proper expressions for $\sin\ \gamma'(t)$ and $\cos\ \gamma'(t)$, the demodulated output obtained is written as

$$Z(\theta) = \frac{4}{\pi}\left[\frac{A + n_c^2}{[(A+n_c)^2+n_s^2]^{1/2}} \cos\theta + \frac{n_s}{[(A+n_c)^2+n_s^2]^{1/2}} \sin\theta\right] \quad (42)$$

The first two moments of Eq (42) are now required to evaluate the SNR. The first moment $u_z$ is defined as

$$u_z = E\{z(\theta)\} = \int_{-\infty}^{+\infty} z\, f_z\, dz \quad (43)$$

while the second moment is defined as

$$E\{z(\theta)^2\} = \int_{-\infty}^{+\infty} z^2\, f_z\, dz \quad (44)$$

These two moments are then used to express the variance as

$$\sigma_z^2 = E[z^2] - E[z]^2 \quad (45)$$

Because it has been assumed that the noise is white Gaussian noise, the evaluation of the expectations yield (Ref 16:43-45)

$$u_z = (2\rho/\pi)^{1/2}\, e^{-\rho/2}\, [I_o(\rho/2)+I_1(\rho/2)] \cos\theta \quad (46)$$

and

$$\sigma_z^2 = 8/\pi^2[\cos^2\theta - (1-e^{-\rho}/2\rho)\cos 2\theta] - u_z^2 \quad (47)$$

Since the input and output SNR are the quantities of interest, these SNR's are given by

$$\left(\frac{S}{N}\right)_0^{\hat{\theta}} = \frac{u_z^2}{\sigma_z^2} \quad (48)$$

at the output of the BPL. The output-input ratio is

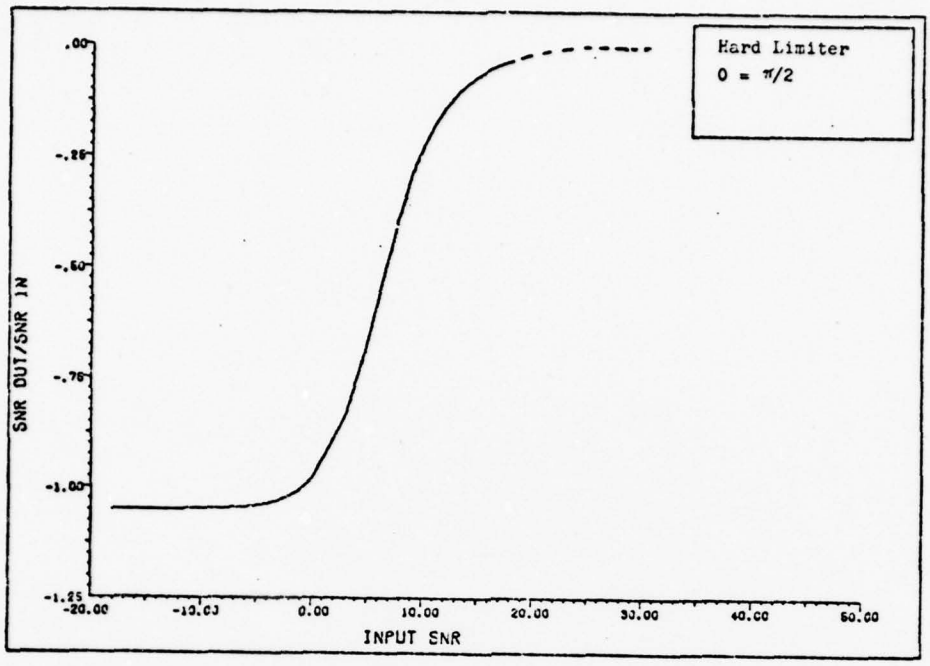


Fig 5. Bandpass Limiter Ratios of SNRs

$$\frac{\left(\frac{S}{N}\right)_0^{\theta}}{2\left(\frac{S}{N}\right)_i} = \frac{u_z^2}{2\rho\sigma_z^2} \tag{49}$$

The bandwidth change of 1/2 is required due to the bandpass to lowpass transformation. The input SNR is $\rho$. Finally, the SNR for the coherent case is a function of $\rho$ when $\theta = 0$ is expressed as

$$\frac{(S/N)_0^0}{2(S/N)_i} = \frac{1}{2}\,\frac{e^{-\rho}[I_o(\rho/2) + I_1(\rho/2)]^2}{(4/\pi)\{1-[(1-e^{-\rho})/2\rho]\}-\rho e^{-\rho}[I_o(\rho/2+I_1(\rho/2)]^2} \tag{50}$$

and when $\theta = \pi/2$ is expressed as

$$\frac{(S/N)_o^{\pi/2}}{2(S/N)_i} = \frac{1}{2} \frac{e^{-\rho}[I_o(\rho/2)+I_1(\rho/2)]^2}{2/\pi[(1-e^{-\rho})/\rho\ ]} \qquad (51)$$

In Fig 5, the relationship between the input-output ratio for $\theta = \pi/2$ is graphically depected. Included in this section are the incoherent and coherent SNR relationships. The complete end-to-end hard-limited channel for a TDMA or an FDMA access with PSK modulation can be characterized by parameters such as $P_e$, SNR, BW, and bit rate.

Soft-Limiter Suppression

The analysis of the soft-limiter follows that of the hard-limiter. Springett and Simon (Ref 16) have found that when a hard-limiter is followed by a coherent detector, the strong signal asymptotic values no longer agree with the incoherent results derived by Davenport. Those results were found to apply equally well to a coherent soft-limiter.

The signal and noise, as previously defined in the preceding section and given by Eq (19), are once again the input. The model for the soft-limiter is given in Fig 6 and replaces the ideal limiter in Fig 4 given by Eq (25). The soft-limiter representation seen in the figure is that for the error function representation.

The narrowband waveform which is represented by Eq (20), when fed to a memoryless non-linear device, yields an output v(t), which is a function of the input. Before proceeding further, the input was written in a more convenient form as

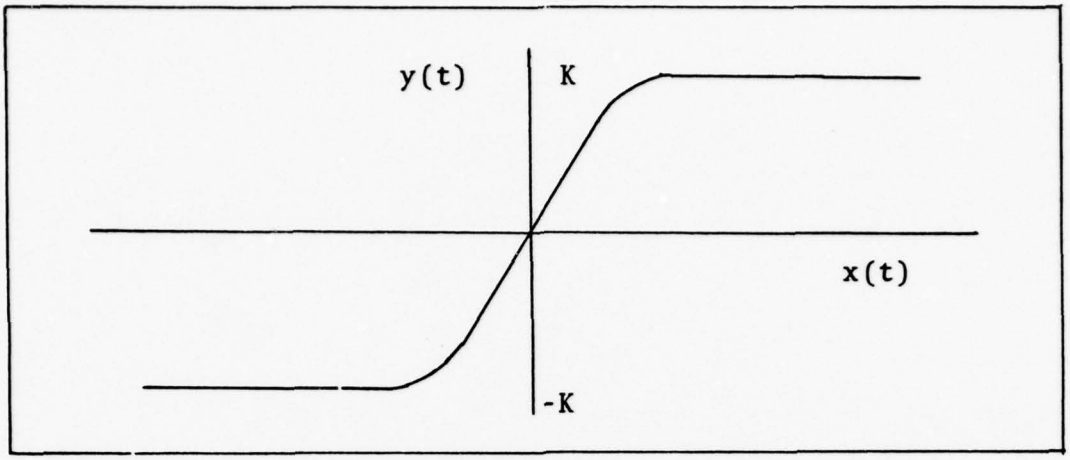


Fig 6. Soft-Limiter Model (Represented by the Error Function

$$x(t) = a(t) \cos[w_c t + \phi + \gamma(t)] \tag{52}$$

The input signal and noise are identical to those given by Eqs (27), (28), and (29). Letting $\alpha = w_c t + \phi + \gamma(t)$, the input is now expressed as

$$x(t) = a(t) \cos \alpha \tag{53}$$

Since the output is an even periodic function of $\alpha$, it is represented by the Fourier series (Ref 2:398-399)

$$v(a \cos \alpha) = 1/2\ v_o(a) + v_1(a) \cos \alpha + \ldots \tag{54}$$

The expansion is valid regardless of how a(t) and $\alpha$ vary in time. The $v_m(a)$ terms of Eq (54) are given by the Chebyshev transform. These terms are called the m-th order of the transform. The first order Chebyshev transform, $v_1(a)$, is the only frequency component that is passed by the zonal bandpass

filter which follows the non-linearity. The variable a(t) is non-negative, and is defined by the expression of Eq (28).

The non-linearity for a soft-limiter is expressed as

$$y(t) = L \text{ erf } \left(\frac{K\pi}{2L}\frac{1/2}{x(t)}\right) \tag{55}$$

where L is the peak limiter output and K is the slope of the transfer characteristic at $x = 0$. Hence, the output of the soft-limiter as determined by Blachman (Ref 8:399) is given by the expression

$$y_1(t) = L\left(\frac{2}{\pi}\right)^{\frac{1}{2}} a e^{\frac{-a^2}{4}} \left\{I_o\left(\frac{a^2}{4}\right) + I_1\left(\frac{a^2}{4}\right)\right\} \tag{56}$$

The independent variable t has been suppressed above. The expression of Eq (56) was numerically evaluated, and those results are provided in graphical form in Fig 7. The amplitude of the signal approaches its maximum value (limit) for SNR>4. At first glance, it appears that the signal exceeds unity, and hence, the output appears to be amplified. However, that is not the case. The amplitude obtained at the output of a hard-limiter must be multiplied by the suppression factor $\pi/4$. Thus, the amplitude reduces to a maximum output value of unity. Consequently, $v_1(a)$ describes the envelope in the fundamental zone. The envelope was determined from the results of Blachman (Ref 2) who made use of the Chebyshev transform to derive his results.

A coefficient must now be introduced, since it was ignored completely in the previous steps. Because the error function

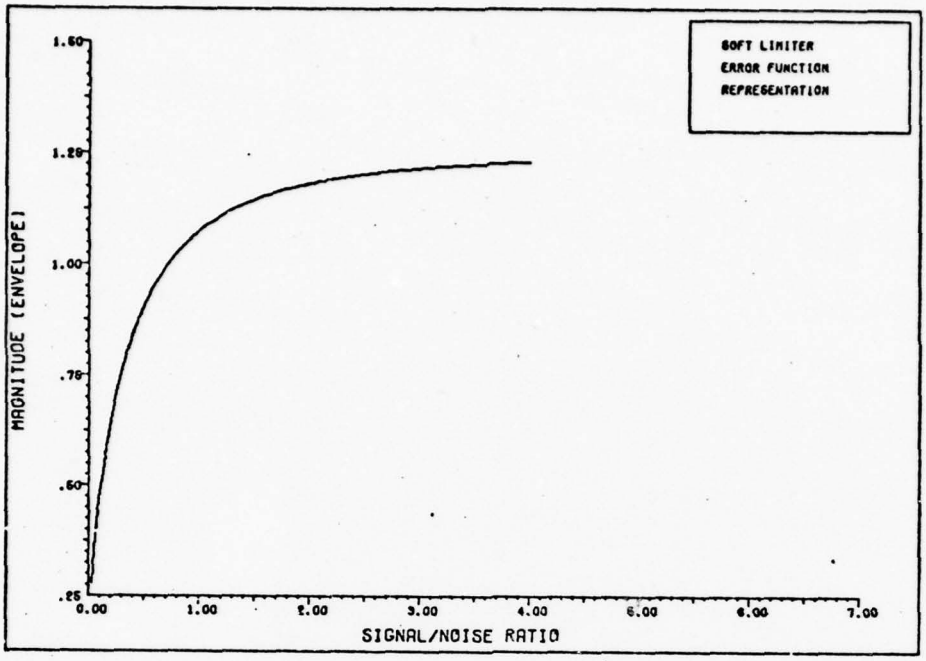


Fig 7. Envelope Magnitude at the Output of the Soft-Limiter versus Input Signal-to-Noise Ratio

was defined with the argument, $[K^{1/2}/2L\ x(t)]$, the coefficient that precedes $x(t)$ must be accounted for. It is obvious that $a(t)$, as previously defined, must be modified to the expression

$$a(t) = \frac{K^{\frac{1}{2}}}{2L} \{[A + n_c(t)]^2 + n_s^2(t)\}^{\frac{1}{2}} \qquad (57)$$

which simply says that the peak value of the limiter and slope at $x = 0$ are variables. They are defined specifically for a specific TWT.

The output $y_1(t)$, which is similar to that of Eq (40), is then multiplied by the coherent reference, $r(t) = \cos(w_c t + \theta)$, and low-pass filtered. After the expressions for $\sin \gamma(t)$ and

cos $\gamma(t)$ are substituted into the resultant output, the output is identical to that of Eq (42), but it must be multiplied by the coefficient $-K^{1/2}/2L$.

The first two moments of the output are required to evaluate the SNR. The first moment $u_z$ is defined in Eq (43), while the second moment is defined in Eq (44). From these two moments, the variance was found using Eq (45). The process used to derive the first and second moments is not summarized here. Instead the reader is asked to read (Ref 9) if he wants that information. Proceeding further and using Lesh's (Ref 9) results, the input-output signal-to-noise ratios for a coherent phase detector is given by

$$\frac{SNR_0^{\pi/2}}{2SNR_i} = \frac{-u_z|_{\theta=0}}{R'\{E[z^2] - u_z^2\}} \tag{58}$$

where $\theta = \pi/2$. R' is the SNR at the input after projection onto the coherent reference axis and is given by

$$R' = 2R \cos^2 \theta \tag{59}$$

which further reduces the expression of Eq (58) to an expression where R' is replaced by 2R.

The behavior of a phase detector with detection angle, $\theta = \pi/2$, is expressed in terms of input-output SNR relationships in Fig 8. The parameter $\beta = L/KA$ in that figure can be interpreted as the ratio of the peak limiter output to the peak signal output, if the limiter is a linear amplifier with gain K. When $\beta = 0$, the error function represents a

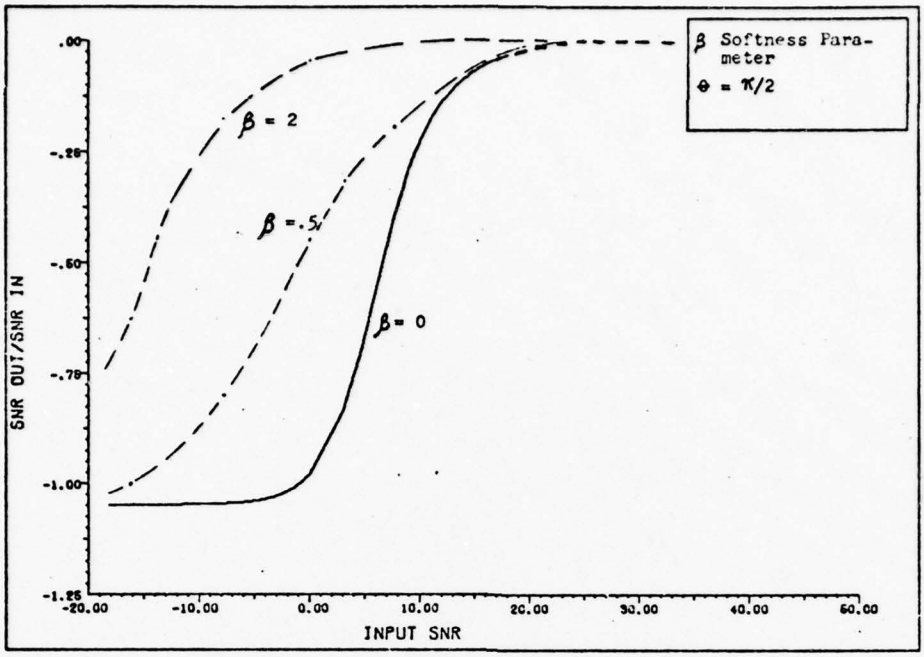


Fig 8. Soft Bandpass Limiter Ratios of SNRs

hard-limiter. The curves in the figure were extracted from another figure found in (Ref 9). The curve for $\beta = 0$ is the actual curve that is generated for a hard-limiter as a function of SNRs. The phenomenon that is depicted by the three curves is obvious. As $\beta$ gets larger, the system behaves as a linear amplifier. As $\beta$ gets smaller, the system behaves as a soft-limiter. The system becomes a hard-limiter when $\beta = 0$.

Spectrum Distortion

The problem under consideration is the amplification of several signals in a common device in which limiting occurs. This problem is of particular importance in satellite communication systems when more than one access is required. The

method which was derived from Rice (Ref 3) and used here in determining the output of a limiter follows that of Davenport and Root (Ref 4:277-311). It consists of computing the autocorrelation function at the limiter output and then taking a Fourier transform to obtain the spectrum. The derivation of the autocorrelation and spectrum is summarized and follows. The Wiener-Khintchine theorem states that the Fourier transform of the spectral density yields the autocorrelation function

$$S_y(f) \leftrightarrow R_y(t_1,t_2) \tag{60}$$

when

$$R_y(t_1,t_2) \equiv R(\tau) \tag{61}$$

Hard-Limiter. The autocorrelation function of the limiter output is defined as the statistical average

$$R_y(t_1,t_2) = E\{g[x(t_1)]\cdot g[x(t_2)]\} \tag{62}$$

where $t_1$ and $t_2$ are two arbitrary times. Since the ideal limiter characteristic as described by Eq (25) can be represented by a sum of contour integrals in the complex plane ($w = u + jv$), the representation is given by (Ref 2:277-282)

$$g(x) = \frac{1}{2}j\pi\{\int_{C_+}\exp(wx)\cdot\frac{dw}{w} + \int_{C_-}\exp(wx)\frac{dw}{w}\} \tag{63}$$

The autocorrelation function of the output y of a non-linear device when the inputs consist of sinusoidal signals plus independent Gaussian noise is given by (Ref 13:511):

$$R_y(t_1,t_2) = \sum_{k=0}^{\infty} R_n^k(t_1,t_2)\frac{1}{(2\pi j)^2} \int_c f(w_1)\ w_2^k \cdot$$

$$\exp\ (\sigma_1^2\ w_1^2\ /2)\ dw_1 \int_c f(w_2)\ w_1^k \cdot$$

$$\exp\ (\sigma_2^2\ w_2^2\ /2\ \ dw_2 M_x(w_1,w_2) \qquad (64)$$

where

$R_n$ = autocorrelation function of the noise

$M_x(w_1,w_2)$ = characteristic function of the input signal

$f(w)$ = bilateral Laplace transform of the characteristic function of the non-linear device

$\int_c$ = integration over the line $w = u - j\infty$ to $w = u + j\infty$

The normalized transfer function for a hard-limiter output is given by Eq (25). The above results have been stated without showing the actual derivation. A complete analysis of the limiter output which culminates with the derivation of the autocorrelation function is documented in (Ref 1).

After considerable manipulation of mathematical equations and analysis of those equations, Shaft (Ref 5) was able to derive the power spectrum by transforming the autocorrelation function. The resulting relationship for the magnitude of the power spectrum at the various frequencies is given by

$$S_{m1\ \ldots mn} = \{\int_{-\infty}^{+\infty} (\frac{1}{x}) J_{m1}(A_1 x)\ \ldots J_{mn}(A_n x) \cdot$$

$$\exp\ (\frac{-\sigma^2 x^2}{2})\ dx\}^2 \qquad (65)$$

whenever $|m_1| + \ldots + |m_n|$ = odd. The terms which have the

largest magnitude are those which satisfy $|m_i|_{max} \leq 2$. The subscripts $m_1 \ldots m_n$ denote the harmonic content of the term under consideration. For example, 100...0 indicates that the term consists of the fundamental of signal (m = 1) and no other term contributes ($m_i = 0$, i = 2...n). Similarly, 210...0 is the intermodulation term consisting of the second harmonic of signal one minus the fundamental of signal two. The condition

$$\sum_{i=1}^{n} m_i = 1 \tag{66}$$

must be satisfied for a term to fall in the first zone.

Soft-Limiter. It was noted by Jones (Ref 8), that if a soft-limiter is used, the exponent in Eq (65) must be replaced by $[(\sigma^2 + a^2)\, x/2]$. The variable "a" describes the slope of the error function, and how fast saturation is reached. The effect of adding a soft-limiter on the average output is, therefore, mathematically identical to adding noise to a hard-limiter, provided that the error function representation can be used for the limiter characteristic.

Approximation. Since Eq (65) is very difficult to evaluate numerically for large n and because there are no close form solutions for n>2, a useful series of approximations can be derived by using the expression

$$\prod_{i=1}^{N} J_o(A_i x) \approx \exp\left(\frac{-\sigma_1^2 x^2}{2}\right) \tag{67}$$

where

$$\sigma_1^2 = \sum_{i=1}^{N} \frac{A_1^2}{2} \tag{68}$$

which was introduced by Gyi and used by Shaft (Ref 14) to produce the magnitude of the desired signals and unwanted signals.

Two Signals. The two signals under consideration are assumed to be of different strength. The hard-limiter output for the strong term is expressed as

$$S_{10} = \{\int_o^\infty \frac{1}{x} J_1(A_1x)\ J_o(A_2x)\ \exp\ (\frac{-\sigma^2 x}{2})\ dx\}^2 \quad (69)$$

The noise in this case was assumed to be negligible. Hence, the exponential term was considered to be unity. After several intermediate steps and a change of variables, $y = A_1x$ , and $dy = A_1dx$ , the output is

$$S_{10} = \{\int_o^\infty \frac{1}{y} J_1(y)\ J_o(\frac{A_2}{A_1}y)\ dy\}^2 \quad (69a)$$

After Eq (14.4.33) from (Ref 1) was used to evaluate Eq (69a), the results obtained were manipulated considerably and give the approximate term for the strong signal output as

$$S_{10} \approx 1 \quad (69b)$$

The strong term receives most of the power from the non-linearity. An approximate expression for the power share of the weak term was derived using the same technique as before. The weak term output is approximately

$$S_{01} \approx \frac{1}{4}(\frac{A_2}{A_1})^2\ S_{10} \quad (70)$$

Its power level is 6 dB below that of the strong term. The

power output of a hard-limiter is divided unequally among the inputs, with the stronger input being allocated a larger share of the power at the expense of the weaker signal.

The general equation for the output from a hard-limiter for two inputs is given by (Ref 14:658)

$$S_{rq} = \left\{ \frac{(A_2/A_1)^q \ [(r+q)/2]}{2\Gamma(q+1)\Gamma[(r-q+2)/2]} \right\}^2 \tag{71}$$

From Eq (71), the intermodulation distortion for $r = 2$ and $q = 1$ is found to be

$$S_{21} = S_{01} \tag{72}$$

Therefore, intermodulation distortion can be obtained and controlled by the proper selection of carrier frequencies. The center frequencies of the carriers are selected in a manner that insures that their intermodulation products fall at frequencies out of the desired zone or where they minimally distort the desired output.

Several Signals. When there are several signals present at the input and no one dominates, the noise term which was previously considered negligible and ignored must now be included. The output term for one of the carriers is given by

$$S_{100\ldots0} = \{\int_0^\infty \frac{1}{x} J_1(A_1 x) \exp\left(-\sigma_2^2 \frac{x^2}{2}\right) dx\}^2 \tag{73}$$

where

$$\sigma_2^2 = \sigma^2 + \sum_{i=2}^{n} \frac{1}{2} A_i^2 \tag{74}$$

The term $\sigma_2^2$ represents noise and those signals whose terms are not of interest are also considered noise and are summed into the noise term as given in Eq (74). After applying Eq (11.4.28) from (Ref 1) the calculated magnitude for the fundamental frequency of the first signal is given as

$$S_{10\ldots0} = 0.7854 \frac{A_1^2}{2\sigma_2^2} \tag{75}$$

which yields a suppression factor of -1.05 dB. This is a well known and well documented result. The magnitude for the other terms at their fundamental frequencies is also given by Eq (73), since each term of the n terms was considered to be equal in magnitude to each individual term in the sum.

Using the approximation introduced and defined earlier in Eq (67), the desired and distortion magnitude terms can be obtained. Those calculated results allow the system designer the choice to select appropriate frequencies to eliminate distortion terms from the fundamental zone or minimize their effect. The total intermodulation power cannot be altered, but it is possible to redistribute it to frequencies where it does no greater harm.

Intermodulation Levels. The crossproducts that are produced when several signals are passed through a hard-limiter are of interest since they represent interfering terms or noise. Values for the magnitudes have been obtained from Eq (65) by Shaft (Ref 13). Shaft presented his numerical results in graphical form. His results were extracted and are

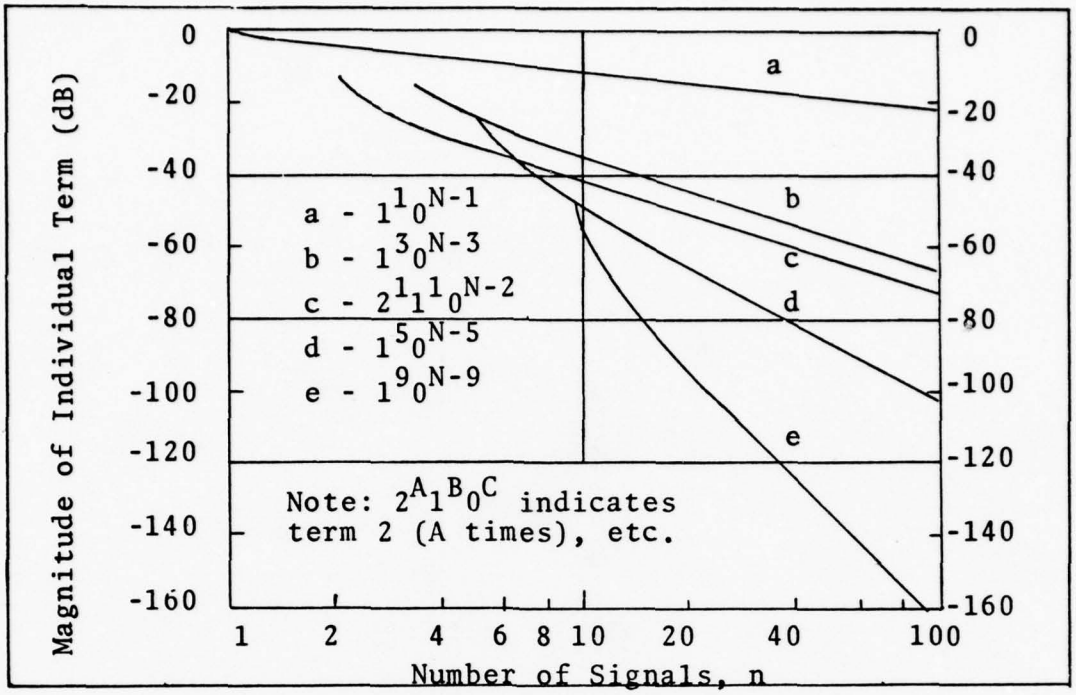


Fig 9. Magnitude of Individual Terms Versus the Number of Signals -n

included here in Fig 9. The magnitudes shown are a function of n signals, all of which have equal amplitude. Several important observations can be noted by careful inspection of the curves in the previously mentioned figure. These observations are as follow: (1) power in an individual term decreases linearly with n; (2) total signal power is approximately one dB less than the total power and remains relatively constant with n; (3) power in an individual term of third and fifth order decrease as $n^3$ and $n^5$, respectively; and (4) bandwidth occupancy for the signals increases linearly with n. Third order terms are defined as

$$\sum_{i=1}^{N} m_1 = 3 \qquad (76)$$

where the $m_i$s are integers which take positive and negative values. Antipodal biphase-modulated signals (BPSK) generate third order (2,1) intermodulation (IM) products which are also BPSK, but whose frequency is offset. Only the dominant intermodulation products are of interest because they occur most frequently and have four times the power of the 210...0 type IM product.

Number of Intermodulation Products. The number of intermodulation products of various orders are tabulated in Table I (Ref 15:243). An approximate analysis was accomplished on a large number of sinusoids to derive the total number of intermodulation products for specific orders. The notation A, B, C,... represents any of the input frequencies. The asterisks indicate the dominant form of the third and fifth order cross-products.

TABLE I

Number of IM Products of Various Orders

| IM Form | Order m | Number of Frequencies | Total Number of IM Products |
|---|---|---|---|
| 2A - B | 3 | 2 | N(N-1) |
| *A + B - C | 3 | 3 | N(N-1)(N-2)/2 |
| 3A - B - C | 5 | 3 | N(N-1)(N-2)/2 |
| *A + B + C - D - E | 5 | 5 | N(N-1)(N-2)·(N-3)(N-4)/12 |

## IV. Detection of PSK Signals

Signals passing through a linear communications channel are corrupted by noise, but their detection is much easier as compared to signals which are passed through a non-linear system that introduces still more noise. The equations that relate the probability of error for making a correct decision for both a linear and a non-linear device are provided in this section. In addition, the probability of error for a hard-limiter and a soft-limiter are found to be expressible by the same equation. However, the softness parameter of the soft-limiter must be taken into account.

### Linear PSK Signal

The problem of communicating one of a set of M specified signals $\{s_i(t)\}$ over a channel which is disturbed by additive white Gaussian noise always reduces to a corresponding vector communication problem. The transmitter signals are represented by M points $\{s_i\}$ in an N-dimensional space. The optimum receiver divides the signal space into a set of M disjoint decision regions $H_i$. At any point, q is assigned to $H_k$ if, and only if, (Ref 18:245)

$$|q-s_k|^2 - N_o \ln P[m_k] < |q-s_i|^2 - N_o \ln P[m_i]$$

$$\text{for all } i \neq k \qquad (77)$$

The signals, as represented in Fig 10, are a binary

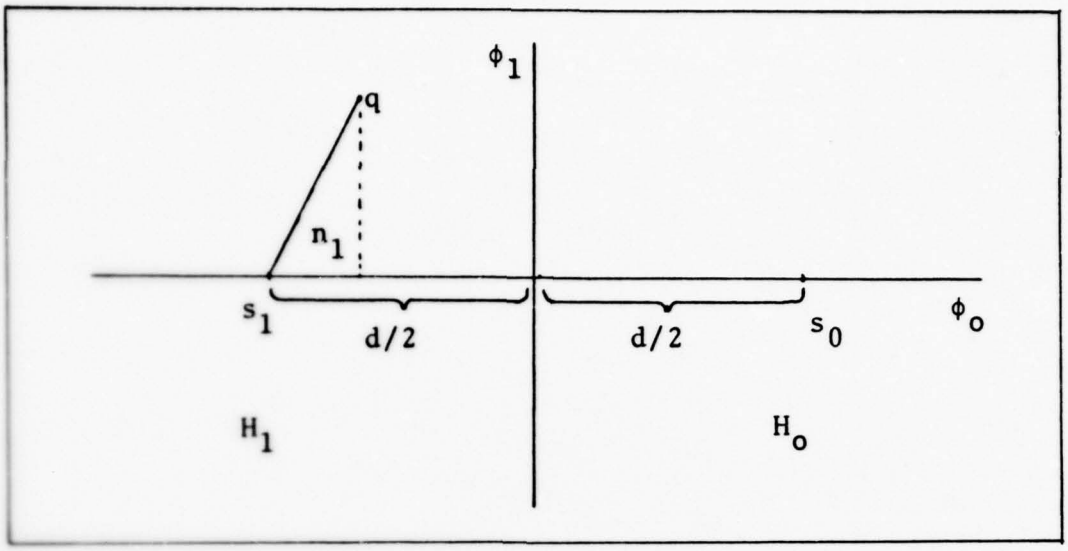


Fig 10. Decision Space for Antipodal Detection

antipodal set. To make a decision, the decision space is divided into two parts by a line perpendicular to $s_1 - s_0$. A complete derivation for binary and M-ary PSK detection is found in Van Tress (Ref 17:254-262), and Wozencraft and Jacobs (Ref 18:245-264). The error probability for antipodal binary signals as given by the above references is

$$P_e = \text{erfc}[(E_b/N_o)^{1/2}] \tag{78}$$

Eq (78) was numerically evaluated. Figure 11 shows those numerical results in graphical form.

Since $s_1(t)$ and $s_2(t)$ have finite energy in time interval -T, their respective energy can be obtained from

$$E_i = \int_{t_o}^{t_o+T} s(t)_i^2 \, dt \qquad i = 1, 2 \tag{79}$$

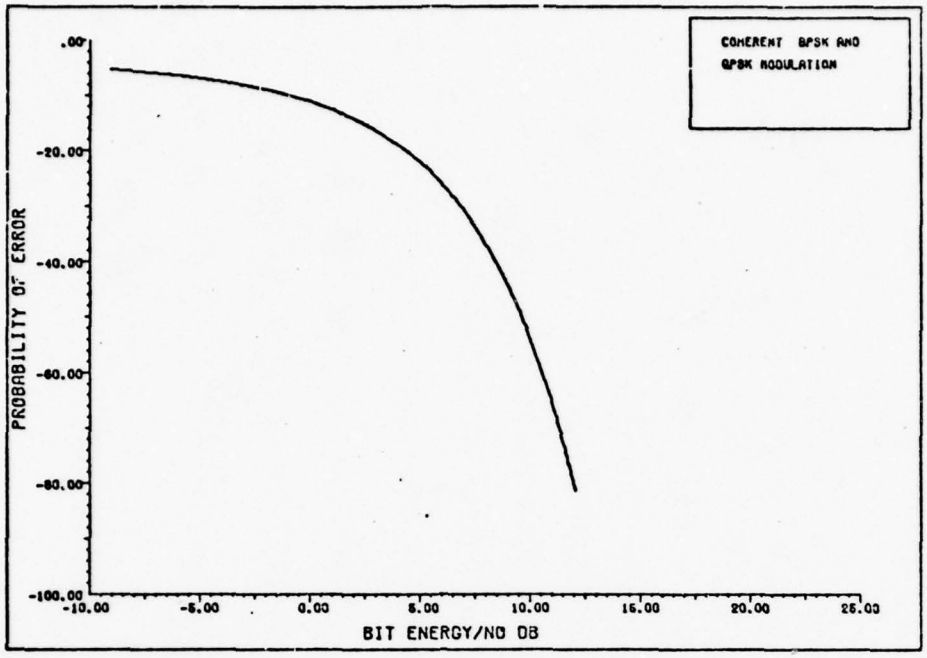


Fig 11. Probability of Error Versus Bit-Energy-to-Noise Density

for antipodal signals, $E_1 = E_2 = A^2T/2$. The energy contained in each signal is identically to the other. For a specific probability of error, the corresponding signal-to-noise density ratio can be obtained from Fig 11 or from Eq (78).

Limited PSK Signal

A binary phased-shift-keyed (BPSK) signal is assumed to get from the transmitter to the receiver via a limiting repeater in the transmission channel. The model for the transmission channel is shown in Fig 12. Additive white Gaussian noise is introduced on both the uplink (repeater noise) and the downlink (receiver noise).

Hard-Limited. The input of the limiter in Fig 12 consists of a binary phase-modulated signal of frequency $w_c$ and amplitude

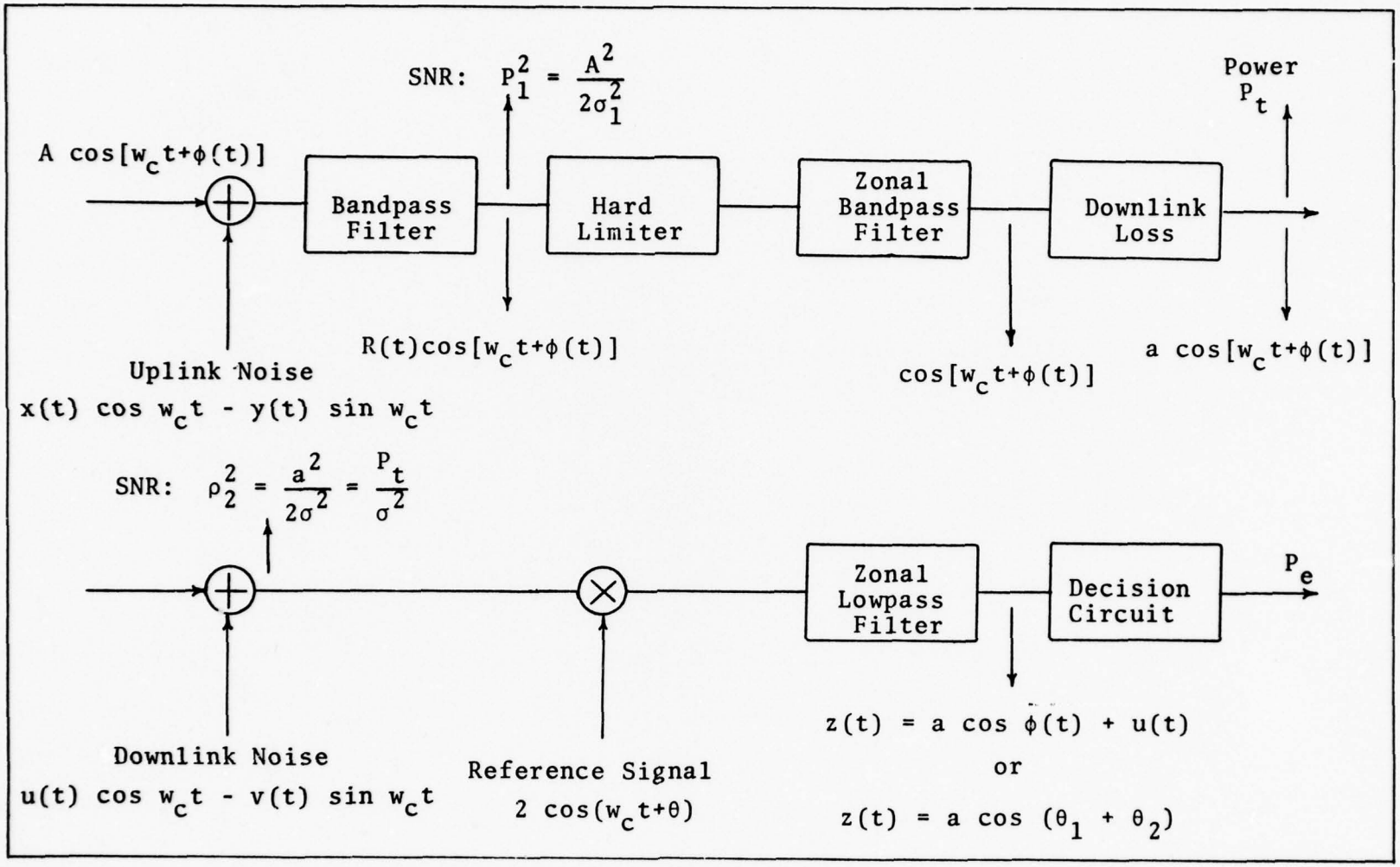


Fig 12. Block Diagram of PSK System

"A" plus zero-mean stationary Gaussian noise of rms value $\sigma$. Two assumptions are made at this point. They are as follows: the noise bandwidth is much smaller than the center frequency of the filter, and the bandpass filter preceding the limiter is wide enough to pass the signal with negligible distortion. The limiter input is as expressed in Eq (27). During any bit interval, the information bearing parameter takes values of either 0 or $\pi$, depending on whether a zero or a one is being sent. The bandpass limiter is assumed to be ideal in the sense that its fundamental-zone output given by Eq (31).

The envelope variations are removed by the limiter, but the phase (which includes the information signal) remains undistorted. The signal is then transmitted to the receiver where noise is added to it on the downlink at the receiver front end. Again, the downlink noise is assumed to be white Gaussian noise and independent of the uplink noise. Hence, the receiver input may be expressed as

$$y_1(t) = a\cos(w_c t+\theta_1) + u(t)\cos(w_c t+\theta_1) - v(t)\sin(w_c t+\theta_1) \qquad (80)$$

where the noise is now referenced to the phase of the information being transmitted. After the signal is multiplied by $2\cos(w_c t)$ and low-pass filtered, the baseband output at the sampling instant is given by

$$z(t) = k(t)\cos(\theta_1 + \theta_2) \qquad (81)$$

where

$$\theta_2 = \tan^{-1}\left[\frac{v(t)}{a + u(t)}\right] \tag{82}$$

and

$$k(t) = \{[a + u(t)]^2 + v^2(t)\}^{1/2} \tag{83}$$

The amplitude of k(t) of the signal is determined by the amplification at the repeater and by the downlink losses. The probability density function of the sum of two statistically independent, identically distributed angles, in this case $\theta_1$ and $\theta_2$, each representing the phase of a sinusoidal signal plus white Gaussian noise, is expressible as (Ref 6:37)

$$f(\theta_i) = \frac{1}{2\pi} + \frac{1}{\pi} \sum_{m=1}^{\infty} \Gamma\left(\frac{m}{2} + 1\right) \frac{\rho_i^m}{m!} \cdot$$

$$ {}_1F_1\left(\frac{m}{2}, m+1, -\rho_i^2\right) \cos m\theta_i \quad \text{for } i=1,2 \tag{84}$$

where $\rho_i^2$ is the signal-to-noise ratio and ${}_1F_1(.)$ is the confluent hypergeometric function.

Error Probability Evaluation. Since the receiver output can be expressed at the sampling instant as the sum of two statistically independent, identically distributed angles as in Eq (81), the probability of error can be determined from the characteristic function and its Fourier transform. The probability density function of the two independent angles is assumed to be of the form $f(\theta) = f(-\theta)$. Also, the probability of a one or zero, which can be represented by different

voltage levels, is assumed equally probable. Each transmitted symbol is statistically independent of its predecessors. Thus, it will be sufficient to determine the error probability of a one or zero since they are equally probable and even symmetric with respect to $\theta$. The probability of error in detecting a one or zero representation is equal to the probability that the receiver output is; let us arbitrarily select negative at the sampling instant. Hence,

$$P_e = \int_{-\infty}^{+\infty} f_z(z)\, dz \tag{85}$$

where $f_z(z)$ is the probability density function of the receiver output z.

To calculate $P_e$, $f_z(z)$ must be determined by first calculating the characteristic function of z and then taking its Fourier transform. Also, the $P_e$ can be obtained directly from the characteristic function. The characteristic function is defined as

$$C_z(v) \triangleq E[e^{-ivz}] = \int_{-\infty}^{+\infty} f_z(z)\, e^{jvz}\, dz \tag{86}$$

from which the density function can be obtained as

$$f_z(z) = \frac{1}{2\pi} \int_{-\infty}^{+\infty} C_z(v)\, e^{-jvz}\, dz \tag{87}$$

If z is any random variable of probability density function f(z) and characteristic function $C_z(v)$, its cumulative distribution function P(x) is (Ref 6:37)

$$P(x) = \int_{-\infty}^{x} f(z)\, dz = \frac{1}{2} - \frac{1}{\pi} \int_{o}^{\infty} \mathrm{Im}[C_z(v)\, e^{-ivx}]dv/v \qquad (88)$$

The probability error was found to be independent of k(t) because the decision is only made on the sign of z. After considerable manipulations, the probability of error as a function of signal-to-noise ratios at the input to the limiter and at the input to the receiver was derived by Jain (Ref 7: 627-628) as

$$P_e = \frac{1}{2}[1 - (1-k^2)^{1/2} \cdot I_e(k,x)] \qquad (89)$$

where

$$k = \frac{\rho_1^2 - \rho_2^2}{\rho_1^2 + \rho_2^2} \qquad (90)$$

and

$$x = \frac{\rho_1^2 + \rho_2^2}{2} \qquad (91)$$

The Rice function written as an integral is

$$I_e(k,x) = \int_{o}^{\infty} e^{-t}\, I_0(kt)\, dt$$

Alternately, the above equation can be represented as a series as

$$I_e(k,x) = \sum_{n=0}^{\infty} (k/2)^{2n}\, (2n)!\, A_n/n!\, n! \qquad (92)$$

where

$$A_n = 1 - [1 + x + \sum_{n=0}^{\infty} x^{2n}/2n!]e^{-x} \qquad (93)$$

Figure 13 was plotted from the numerical results which were obtained from evaluating Eq (92). The probability of error is plotted versus the signal-to-noise ratios at the limiter and receiver input. The numerical results obtained from Eq (92) do not agree with the results obtained by Jain (Ref 7: 627). The two graphs do resemble each other to a large extent. Their disparity is most obvious at the lower values of error probability. It appears that the graph of Fig 13 gives values of one error for every two predicted by Jain's graphical results. Further study of this problem was not carried out because it was determined that the discovery as to the probable cause of the disparity would not provide significant insight into the actual problem being investigated in this paper.

Soft-Limited. Figure 12 will once again be used as the system model, but now the limiter is soft. A soft-limiter and its characteristics have been previously defined by Fig 6. The analysis of a soft-limiter parallels that of a hard-limiter. The results obtained are similar and are summarized in this section.

After the signal is multiplied by the correctly phased reference signal and low-pass filtered to remove the double frequency components, the filter output is

$$z(t) = d \cos(\theta_1 + \theta_2) \tag{94}$$

where

$$d = \{[v_1(a) + u(t)]^2 + v^2(t)\}^{1/2} \tag{95}$$

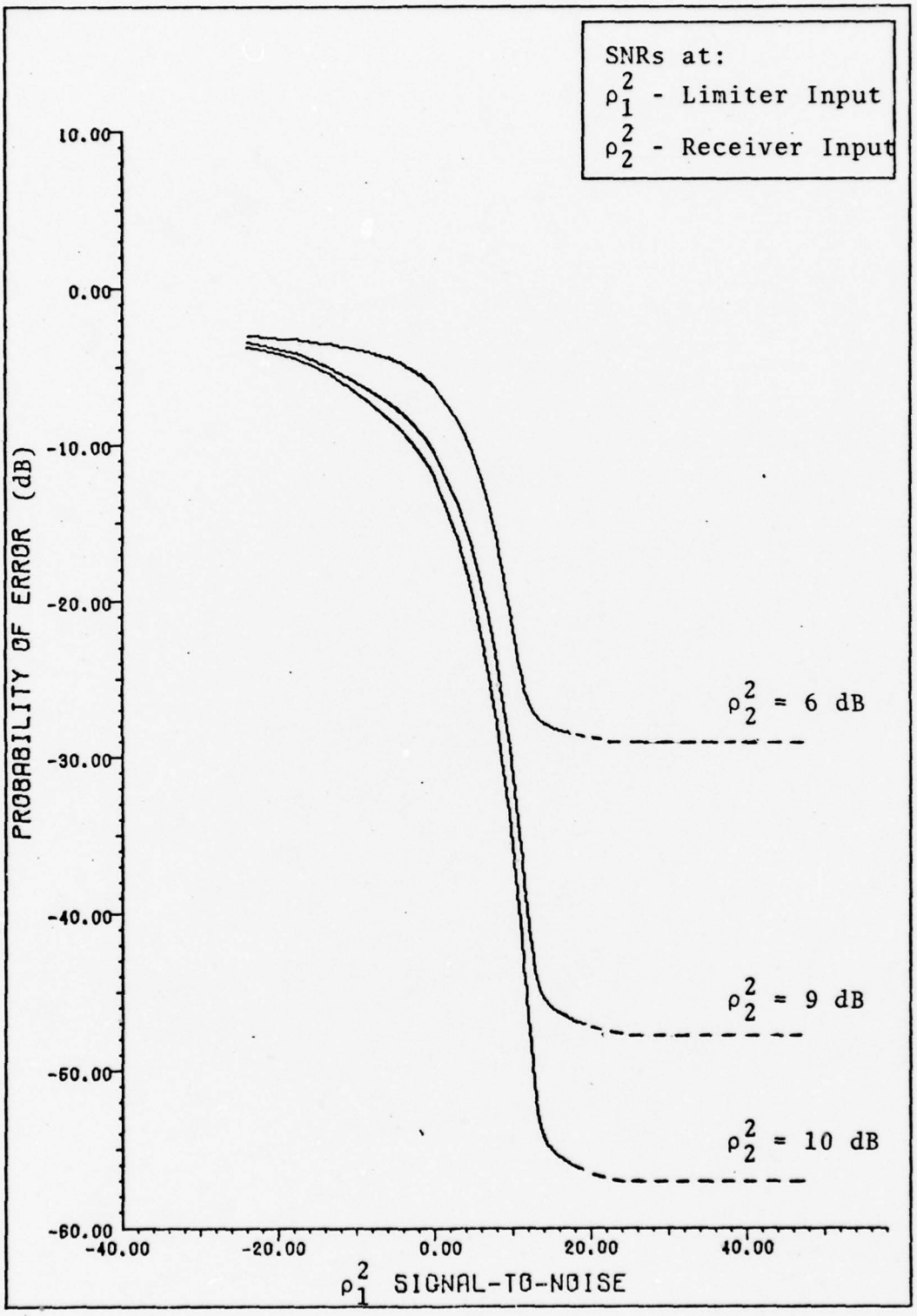


Fig 13. Probability of Error Versus SNR

The amplitude of "d" of the received signal is additionally altered by the amplification in the repeater and the downlink losses after the repeater.

Error Probability Evaluation. Since the receiver output can be expressed at the sampling instant as the sum of two statistically independent, identically distributed angles as in Eq (81), the probability of error can be determined from Eq (89). It is, therefore, obvious that the hard-limited and soft-limited channel are both characterized by the same expression.

Once the signal-to-noise ratio has been determined, the curves which were calculated for the hard-limiter for different probabilities of error are also used for the soft-limiter. At small SNRs, the curves shown in Fig 2 of (Ref 7:627) indicate that the hard-limited channel yields error probabilities which exceed those of a linear or soft-limited channel. However, a very small variation in the signal-to-noise ratio in that region results in a drastic change in the $P_e$. For large SNRs, the advantage of the hard-limiter no longer exists.

## V. Link Calculations

A communications link, which employs dedicated satellite channels of a multi-channel transponder for data transfer, is limited in transmission capability by one of several constraining factors, one of which usually dominates. These factors are as follows: (1) earth station uplink power; (2) satellite downlink power; (3) satellite and earth terminal noise levels; (4) channel bandwidth. The major dominant constraining factors are most often the channel bandwidth or downlink SNR. The equations which make use of the above mentioned parameters characterize a communications system.

### Communications Equations

The design of any telecommunications system makes use of the communications equations which are stated below (Ref 10: 8-15).

$$\frac{P_{rec}}{N_o} = P_t G_t \left(\frac{\lambda}{4}\, d\right)^2 L_0 L_p G_r \frac{1}{KT} \tag{96}$$

$$\frac{S}{N_o} = (1 - L_m) \frac{P_{rec}}{N_o} \tag{97}$$

$$\frac{P_c}{N_o} = L_m \frac{P_{rec}}{N_o} \tag{98}$$

where

$L_0$ = Antenna Pointing Loss

$L_p$ = Polarization Loss

$P_t$ = Total Transmitted Power

$L_m$ = Modulation Loss

$G_t$ = Transmitter Antenna Gain

$G_r$ = Receiver Antenna Gain

$\lambda$ = Wavelength of r-f Carrier

$A_t$ = Antenna Capture Area

Most often, the noise $N_o$ is referenced to the input stage of the receiver. The noise as referenced to the input at the satellite repeater and the earth terminal receiver are quite different values. Usually the noise at the earth terminal receiver is far less than at the satellite receiver. The parameters K and T are defined as

$$K = 1.38 \times 10^{-23} \text{ W/Hz -°K} \tag{99}$$

known as Boltzmann's constant, while T is given in degrees Kelvin. The remaining parameters used in the communications equations are defined as follows:

$S/N_o$ = Received signal-to-noise spectral density ratio in the data channel

$P_c/N_o$ = Carrier signal-to-noise spectral density

$(\lambda/4\pi d)^2$ = Space loss ; where $d \approx 3.563 \times 10^4$ Km

Performance Parameters

The block diagram of a PSK system which, in this case, is considered to be communications satellite path, is shown in Chapter IV, Fig 12. The transmission begins from an earth station, is radiated through space to the satellite repeater,

is amplified and translated in frequency at the repeater, and is finally re-radiated through space to another earth station. Noise corrupts the signal on the uplink and downlink paths. Not only does the transmission suffer corruption from noise sources and path losses, but it must also compete with other transmissions for a share of the total satellite power. As has been stated before, the stronger signals receive a larger share of the total satellite power at the expense of the weaker signals. The disparity can be as high as 6 dB.

The critical parameter to be calculated is the ratio of received carrier power-to-noise density $C/N_o$. The required $C/N_o$ for a given bit rate $R$ is related to the $Eb/N_o$ (energy-per-bit-to-noise density) by the expression (Ref 15:176)

$$\left(\frac{C}{N_o}\right)_{\text{required}} = \frac{E_b}{N_o} + R + M \quad \text{dB-Hz} \tag{100}$$

where R is the bit rate of the information being transferred, and M is almost always fixed at 6 dB as a link margin for X-band operation.

Uplink. The signal power at the satellite input is given by

$$P_s = P_t G_t G_s (\lambda/4\pi d)^2 \tag{101}$$

where

$P_t$ = Earth station transmitter power

$G_t$ = Earth station Antenna Gain

$G_s$ = Satellite Receiver Antenna Gain

The factor $(\lambda/4\pi d)^2$ is commonly referred to as the free space

loss. The antenna gain expression is

$$G_n = \eta 4\pi \frac{A_n}{\lambda^2} \tag{102}$$

where n denotes an arbitrary antenna and $A_n$ an arbitrary aperture. The efficiency $\eta$ is normally .55 for a parabolic reflector operating in the X-band. The noise level at the satellite input is expressed as

$$N_o = KT \tag{103}$$

Thus, the carrier to noise spectral density is of the form

$$\frac{P_s}{N_o} = P_t G_t G_s (\lambda/4\pi d)^2 / KT \tag{104}$$

A complete uplink relationship is stated for the signal to noise spectral density by Eq (104).

Downlink. The signals, as they pass through the non-linearity, are altered significantly and have a different power-sharing relationship at the output. Hence, $\gamma$ is introduced here to represent the suppression or enhancement a particular signal experiences. The signal power at the earth station receiver input is obtained from

$$P_R = P_t G_t G_s (\lambda/4\pi d)^2 \tag{105}$$

where the symbols are as previously defined since the antennas used to receive and transmit are, in most instances, one and the same at the satellite and earth station. However, Eq (105) must be altered to include a suppression factor and some amount

of re-radiated noise. The signal and noise passing through the repeater and amplified can be expressed as

$$\text{Signal Power} = \gamma \cdot \text{EIRP}\ (P_s/P_s+KT) \tag{106}$$

$$\text{Noise Power} = \gamma \cdot \text{EIRP}\ (KT/P_R+KT) \tag{107}$$

where $\gamma$ is the suppression factor and EIRP is the power of the repeater output amplified by the antenna gain. Hence, the receive power is

$$P_R = \gamma \cdot G_s P_{ts} P_t (\lambda/4\pi d)^2 \cdot (P_s/P_s+KT) \tag{108}$$

where $P_{ts}$ is the radiated power from the satellite. The noise level at the earth station receiver consists of re-radiated noise and downlink noise and is given by

$$N_R = \gamma \cdot G_s P_{ts} (\lambda/4\pi d)^2 (KT/P_s+KT) + KT' \tag{109}$$

where T' is the noise temperature referenced to the receiver input. Normally, the first term of $N_R$ is very small. In the same manner that the desired signal suffers a path loss, so does the unwanted re-radiated signal. $N_R$ is the sum of two independent white Gaussian noise sources. The satellite link is said to be limited whenever the noise dominates. The more common situation is the downlink-limited channel where the satellite EIRP is the limiting factor. The carrier-to-noise density for that specific case is approximated as

$$\frac{P_R}{N_R} \approx P_{ts} \gamma P_t G_s (\lambda/4\pi d)^2/KT' \tag{110}$$

The parameter $\gamma$ takes into account such factors as power sharing and suppression. In effect, $\gamma$ represents the share of the satellite power a particular signal receives in the competitive environment of several signals.

## VI. Configuration Analysis

To understand how a system functions with an input of several signals which are not all of the same amplitude and information carrying capacity, it was first necessary to analyze the performance of the system with only one access. Then, the system was analyzed with several inputs, all of which were identical in bandwidth requirement and amplitude. Those results have been previously derived and summarized in the preceding chapters. In this chapter, those results are combined in an effort to understand the degraded performance of the system when several signals of different amplitudes and information bearing capacity interact as they pass through the non-linear repeater. The FDMA/PSK access, when $\phi$ takes values of 0 and $\pi$, are found not to approach a Gaussian distribution and found, therefore, not to appear as Gaussian noise, regardless of how many signals are taken into the sum. That analysis was accomplished to establish a lower bound on the suppression factor. However, the result turned out to be the upper bound. The least suppression a signal experiences in the presence of several FDMA/BPSK signals is 1.05 dB. In reality, the suppression factor will always be greater than that. FDMA/PSK signals with $\phi$ varying uniformly between $-\pi$ and $\pi$ do approach a Gaussian distribution. The FDMA/PSK signals suppress the TDMA signal by at least 1.05 dB and much more. In turn, the TDMA signal and n-1 FDMA/BPSK signals

suppress the n-th FDMA signal by at least 1.05 dB. The suppression that each of the signal experiences is related to their individual power. Most signals are suppressed by up to 6 dB.

Time Division Multiple Access

In TDMA, the signaling waveforms are orthogonal in time because each terminal has exclusive use of the satellite during periodically recurring time intervals or slots. The slots and slot assignments are not considered or discussed here since it has been assumed that those problems will be solved in the design of the TDMA equipment and subsequent to this study.

Because each earth terminal transmits and receives information to and from the satellite in separate non-overlapping time slots, the generation of intermodulation products in the non-linear device is avoided. However, a hard-limiter does introduce some signal suppression. The greatest suppression is -1.05 dB for very small SNRs and 0 dB for large SNRs, as has been previously calculated and as shown in Fig 5.

Moreover, the TWT is operated at maximum output to take full advantage of the limited and precious satellite power. The complete end-to-end communications channel for a hard-limited or soft-limited TDMA/PSK communications channel can be accomplished with the aid of Figs 5, 8, and 11, or the equations which were used to generate the graphs for those figures. It was determined that the limiting factor for a single TDMA access for a specific

probability of error was the satellite power and not the channel bandwidth. A link calculation was accomplished to illustrate this point and is provided in tabular form in Table II. Also, the most information that can be effectively transmitted through a 60 MHz channel was found to be 30 Mb/s for BPSK and 60 Mb/s for QPSK. Figure 14 shows three accesses at the operating frequency and bandwidth of the DSCS III transponder II. The accesses, as they appear in the frequency domain, are indistinguishable from each other except for the bandwidth requirements. Figure 14a shows two accesses which could be considered to be FDMA and one access which could be considered TDMA. It should now be obvious that FDMA and TDMA with phase shift modulation have the same frequency spectrum. However, the TDMA access will almost always have a wider frequency spectrum. Again, looking at the figure closely reveals that the three accesses have identical power. That is, if the area under their respective curves is somehow calculated by some integration scheme, they will all have the same value. The spectrum with the wider bandwidth will, of course, yield a lower energy-per-bit term since more information is being transferred by that access. The figure just below the previously discussed one shows two interesting phenomena. (1) The energy-per-bit for each of the three signals is now identical. The individual power in each of the r-f carriers was adjusted to insure that each bit received the same power ratio as for the access with less information bearing capacity. (2) The spectral density of the largest

TABLE II

Link Calculation for a Single TDMA Access

| | | | |
|---|---|---|---|
| **Uplink Calculations** | | | |
| EIRP (dBW) | 43.7 | to | 73.7 |
| $G_s$ (dB) | | | 29.0 |
| System Losses (dB) | | | -3.0 |
| Free Space Loss (dB) | | | 201.7 |
| Received Signal Level (dBW) | -129.0 | to | -99.0 |
| Noise Density (dBW/Hz) | | | -195.6 |
| Carrier Power to Noise Density (dB-Hz) | 66.6 | to | 96.6 |
| **Downlink Calculations** | | | |
| EIRP (dBW) | | 39, 43, | 45 |
| $G_t$ (dB) | | | 43.7 |
| Free Space Loss (dB) | | | 202.3 |
| Received Signal Level (dBW) | | | -113.6 |
| Noise Density (dBW/Hz) | | | -202.9 |
| Carrier Power to Noise Density (dB - Hz) | | | 89.3 |

**Carrier Power to Noise Density (Required)**

For an error probability $P_e = 10^{-5}$ with Binary phase shift keyed - $E_b/N_o = 9.6$ dB

$C/KT = R + E_b/N_o + M$

**Information Rate and Bandwidth Requirements**

$R = 89.3 - 9.6 - 6.0 = 73.7$

$R = 23.44$ Mb/s

Bandwidth = 46.88 MHz

Available Transponder Channel Bandwidth = 60 MHz

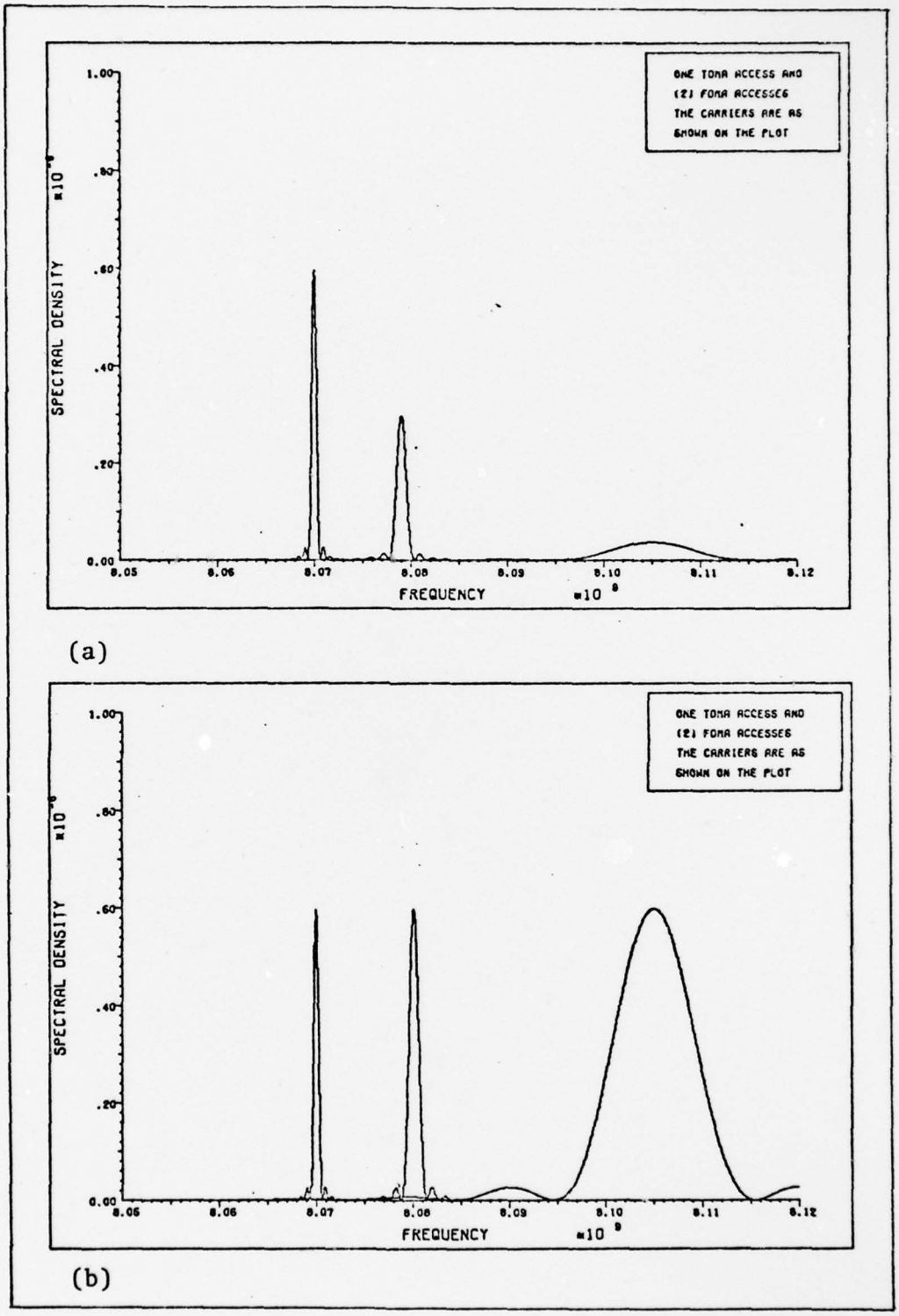


Fig 14. Multiple Access Representation in the Frequency Domain, (a) Unequal $E_b/N_o$ for each the Three Accesses, (b) Equal $E_b/N_o$ for each of the Three Accesses

access overlaps into the frequency space of the other two accesses. That distortion is crosstalk into the other accesses and results in degraded performance.

Simultaneous Multiple Accesses

In the following section, an attempt was made to prove that a satellite system which includes one TDMA access and several FDMA accesses can, in most cases, be modeled as a hard-limiter. It is known that TDMA bursts occur intermittently. That is, each terminal is allocated a time slot for transmission by some control method, but that does not guarantee that some slots will not remain vacant. With knowledge of such occurrences, it was possible to analyze the output spectrum of the BPL with the TDMA access active and inactive. When the TDMA access is inactive, the FDMA accesses have complete use of the satellite power. It should be remembered that the TDMA access vacancies or inactive slots occur very infrequently, but they do occur. How the output power of a BPL is shared by n accesses of equal magnitude at the input to the repeater has been determined in previous chapters.

The main problem under consideration was the analysis of simultaneous non-homogeneous multiple accesses sharing the limited satellite power. The nature of TDMA communications required that the access drive TWT into saturation. It is necessary to operate at saturation to maintain a uniform output because of the many users that contribute data for transmission through the satellite during each second. The users, by some control method which is not of concern here, are

assigned and removed from the system on a random basis, based upon user priority and availability of slots for data transmission.

System Model. The system model for several accesses, which includes a TDMA access and several FDMA accesses, is shown in Fig 15. The n individual signals are competing for a share of the satellite power. Their interaction through a piecewise limiter was analyzed. The limiter representation is shown in Fig 16. Whenever the signal and noise components exceed e, the output of the limiter can be considered identical to that of a hard-limiter as given by Eq (25). It is, therefore, apparent that whenever the magnitude does not exceed e, the limiter will be operating in the soft region and can be considered a linear amplifier of gain K.

Normally a TWT operates as a soft-limiter when its operating point is backed-off $\beta$ dB. $\beta$ is usually adjusted to 3 dB or more for FDMA operation. The result is lower intermodulation products, but the drive level of the n signals must be carefully controlled. For large fixed ground terminals, accurate uplink power control is feasible. For mobile tactical terminals, it may prove exceedingly difficult, if not impossible, to keep the aggregate drive level to the limiter at the proper point.

Piecewise Limiter. The clipping effect of the linear piecewise limiter was determined by Spilker (Ref 15:232). When the input A does not exceed e, the output is $B_1 = A$. For A > e, the peaks of the sinusoid drive the limiter into

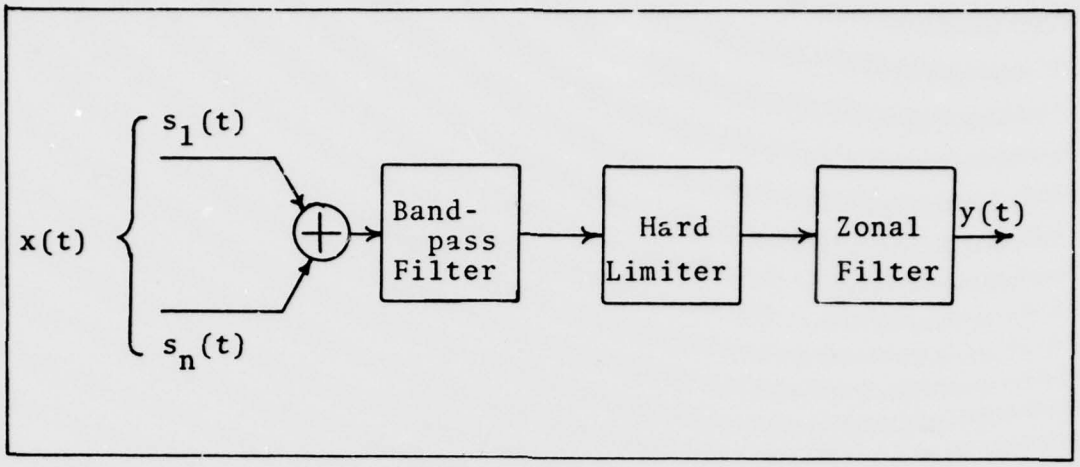


Fig 15. System Model for Several Accesses

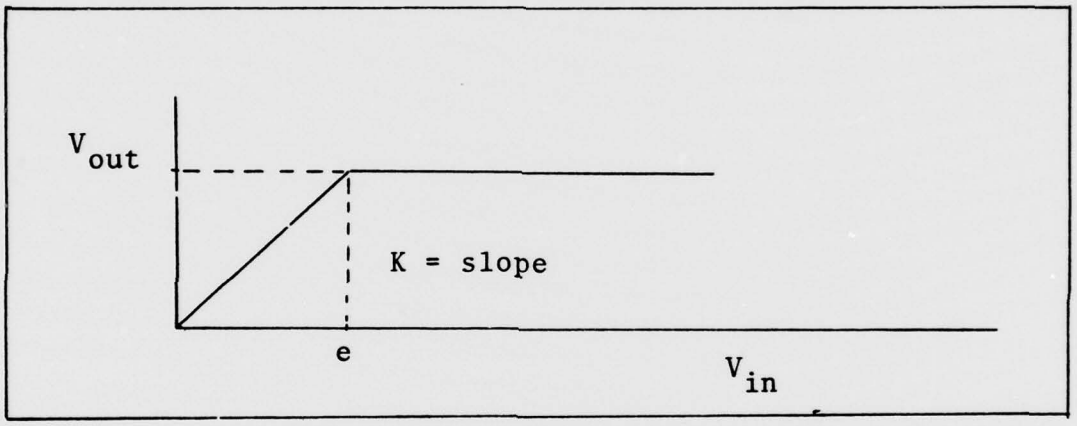


Fig 16. Soft-Limiter (Represented by Piecewise Limiter)

saturation and appear clipped off at the output. The output is, therefore, the sum of the contributions from the limiting and from the linear regions. Thus, the output is given as

$$B_1 = \frac{2e}{\pi} \{[(1-(\frac{e}{A})^2]^{1/2} + \frac{A}{e} \sin^{-1} \frac{e}{A}\} \qquad (111)$$

The magnitude of the output resembles that of the error function limiter which is graphically shown in Fig 7. Whenever the

signal power is much greater than that of the noise, the limiters mentioned above operate very much like hard-limiters.

Signal Suppression. The suppression factor experienced by one sinusoidal signal, which can be the sum of n weak signals, in the presence of a strong sinusoid has been found to be 6 dB. Also, the suppression factor experienced by the weak sinusoid decreases to 1.05 dB when the strong signal has a Gaussian probability density. These two cases are the most and least a sinusoid can be suppressed, respectively. These results have been derived in the hard-limiter suppression section and are in complete agreement with Spilker's results (Ref 15:226).

For two sinusoidal inputs with envelopes $A(t) = A$ and $B(t) = B$, the weak signal B is suppressed by 6 dB. The weak signal B is suppressed by a factor of 2 in amplitude and a factor of 4 in power. This suppression factor is valid even when the weak signal is composed of the sum of a large number of sinusoids.

For a strong Gaussian interference and a weak sinusoid, the suppression factor is 0.7854 (Ref 15:226-227). The result, as stated, applies to the case of n FDMA accesses. Each and every individual access plays the role of the weak signal and is suppressed with respect to the total output power by the suppression factor -R.

A configuration, which consists of several FDMA accesses and one TDMA access, was considered to approximate a Rician interference which consists of a Gaussian noise source and a

sinusoid. The FDMA accesses were taken to represent the Gaussian noise; the TDMA access was taken to represent the sinusoid. The Rician probability density is given by (Ref 15:229)

$$f(A_n) = A_n \, e^{-(A_n^2+2r)/2} \, I_0[(2r)^{1/2} \, A_n] \qquad (112)$$

where $r = P_c/P_n$ which is the power ratios of the fixed envelope interference sinusoid to the Gaussian noise. The Rician density is graphed in Fig 17a for various SNRs. The factor that a sinusoid experiences in the presence of the noise through a bandpass hard-limiter can be computed from

$$R = \frac{\pi}{4} \, (1+r)[e^{-r/2} \, I_0(\tfrac{r}{2})]^2 \qquad (113)$$

which was also numerically evaluated. The results obtained are presented in graphical form in Fig 17b. As expected, the suppression factor varies between a minimum value of 1.05 dB and a maximum value of 6 dB. As stated earlier, a weak signal in the presence of a white Gaussian noise source suffers the least suppression while it suffers the most suppression in the presence of a strong sinusoid.

Gaussian Approximation. It was necessary at this point to prove that the sum of several FDMA accesses with binary phase modulated information impressed on them do constitute Gaussian noise. To do so, it was first assumed that $x(t,\phi)$ is a stochastic process which can be represented as

$$x(t,\phi) = A_i \cos(w_{ci}t + \phi_i) \quad i = 1,\ldots n \qquad (114)$$

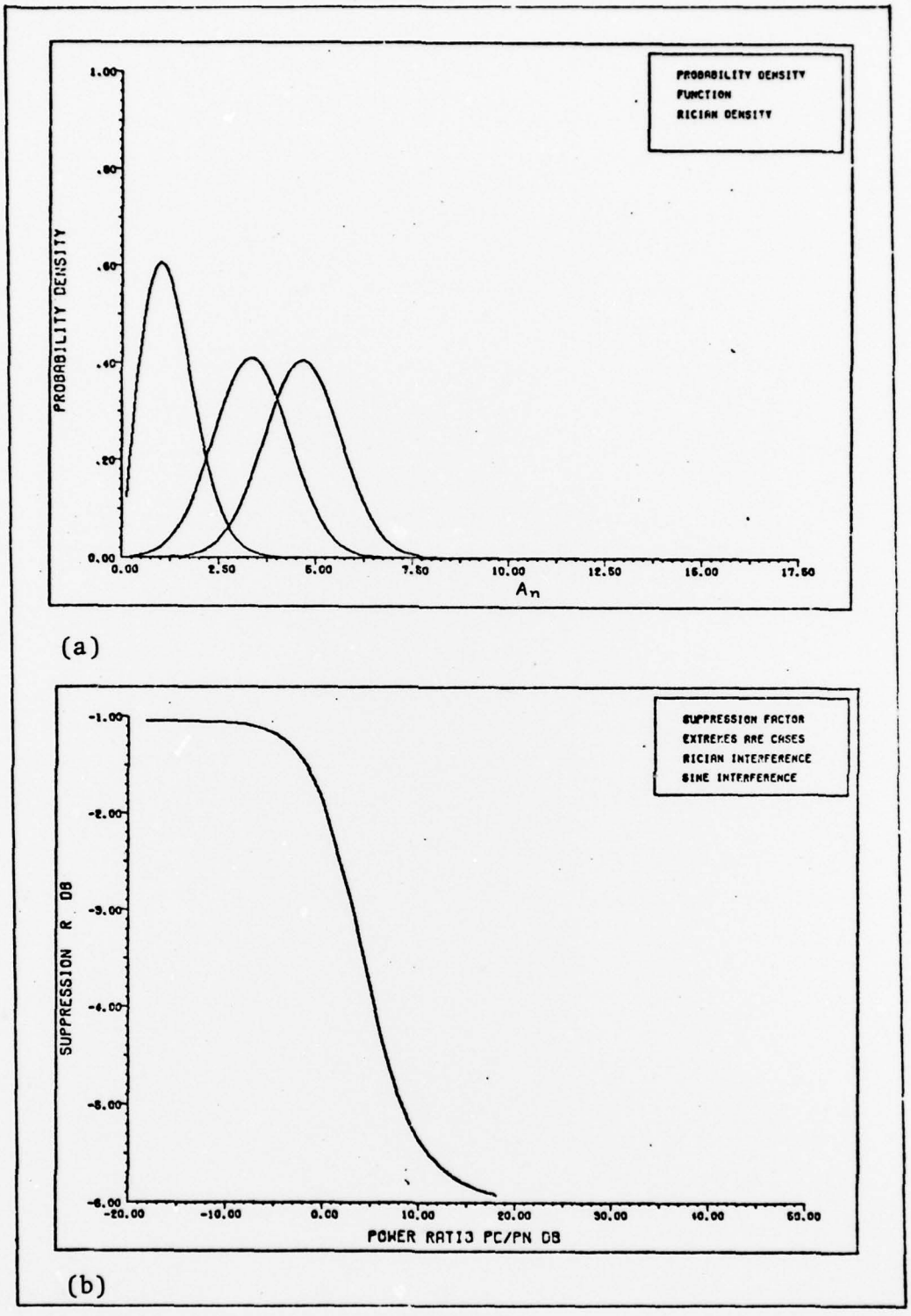


Fig 17. Rician Interference, (a) Probability Density Function vs. SNR, (b) Suppression Factor vs. SNR

where A is the peak value of the ith access and $\phi_i$ is the information bearing variable. The information variable, $\phi_i$, was assumed to take the values, 0 and $\pi$, with equal probability. Hence, the first order probability density of the process was found to be as represented graphically in Fig 18. Hence, $E[x(t)] = 0$, while the variance of x(t) was found to be $\alpha_i^2 = |A \cos w_i t|^2$. It is now possible to represent the sum of the random process as

$$z(t) = \sum_{i=1}^{N} x_i(t) = A \sum_{i=1}^{N} \cos(w_{ci} t + \phi_i) \qquad (115)$$

where the A's are equal in magnitude, and $\phi_i$'s are identically independently distributed random variables with pdf as previously defined.

For a fixed t, the first order pdf of the new process can be found by invoking the Central Limit Theorem. Therefore, the process z for a fixed t has mean and variance defined as

$$z = z(t)|_{\text{fixed } t} \sim N(0, A^2 \sum_{i=1}^{N} \cos^2 w_{ci} t) \qquad (116)$$

The variance was found from the sum of the individual variances of $x_i$'s. Because $x_i$'s are orthogonal with zero mean, then they are also uncorrelated.

Faulty Approximation. The analysis as accomplished in the preceding section to approximate Gaussian noise with n FDMA accesses was erroneously based on the Central Limit Theorem. A closer look reveals that in lieu of the Central Limit Theorem, the Chernoff bound should have been applied.

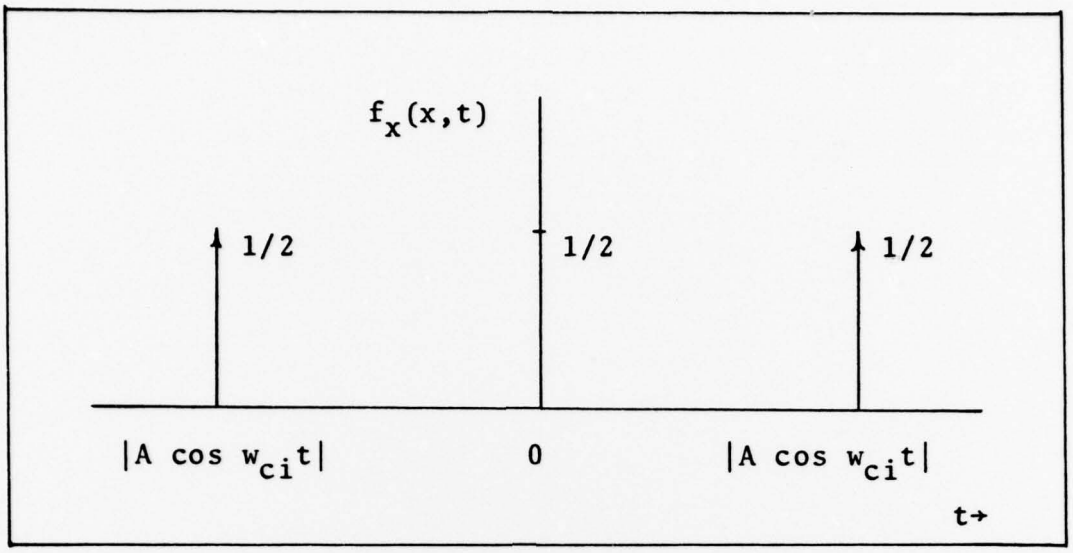


Fig 18. Probability Density of the Stochastic Process -x

Using the Chernoff bound, it was proved in (Ref 18:108-109) that the sum of n random processes which represent BPSK modulated r-f carriers do not approach a Gaussian distribution regardless of how many terms are considered into the sum. A specific case was considered to prove the aforementioned point. N binary random variables were considered in which each assumes the value of 0 or 1 with equal probability. The difference between the values for the approximation and the exact expressions was found to be expressed by an exponential function of N. The fractional error was found to become larger as N became larger. Therefore, the sum of n BPSK modulated r-f carriers do not become Gaussian regardless how many terms are considered into the sum.

Without doubt, it has been proven that the sum of several FDMA accesses will never appear as Gaussian noise.

Hence, the FDMA signals will experience a suppression factor which approaches 6 dB. The suppression factor experienced by the TDMA signal in the presence of several FDMA signals can be found by computing the ratio - $P_c/P_n$. A specific suppression value is obtained from Fig 17b for a specific signal-to-noise ratio.

Non-homogeneous Multiple Accesses

A method to utilize more of the unused transponder channel bandwidth is outlined below. This method is an approximation, but it does serve its purpose well when applied to the environment of several accesses, all of which are homogenous with the exception of one. Figure 19 shows how more use can be made of a channel when the TDMA access does not make complete use of the channel and when the satellite power can support more accesses. The frequency of the FDMA carrier closest to the TDMA access is found from the following equation

$$f_2 = f_1 - 3\Delta f \tag{117}$$

where

B = Transponder Channel Bandwidth

$f_1$ = Carrier Frequency of TDMA access

$f_2$ = Carrier Frequency of FDMA access closest to the TDMA access

$\Delta f$ = Phase Modulation rate of the TDMA access

Approximately one-fifth of the bandwidth can be used for the FDMA accesses. The channel configuration must be as

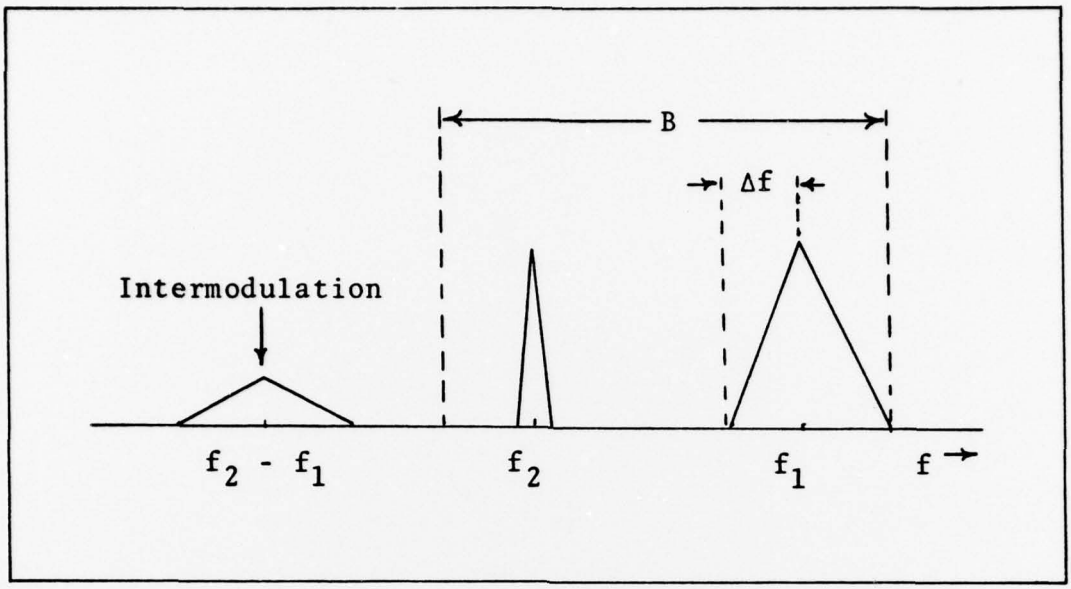


Fig 19. Frequency Separation to Minimize Intermodulations on the Desired Frequency Spectrum

depicted in Fig 19. The dominant intermodulation products fall outside the desired frequency spectrum. Hence, the noise terms of the intermodulation products are placed at frequencies where they do no greater harm.

# VII. Conclusion

The essential background information and facts for the analysis of the problem are included in this report and summarized in this chapter. A recommended solution is provided, although the sponsoring organization is provided with sufficient facts to evaluate other solutions. First, the proposed use of the system is restated. Basically, Hq AFCS desires to implement, if it is deemed feasible, the use of simultaneous non-homogeneous accesses through a common transponder channel.

## Summary

Technology has progressed to the point where it is now feasible to design TDMA equipment that fully utilizes the entire power and bandwidth of a single transponder channel such as that of the DSCS III communications satellite channel II. A link calculation was presented in Chapter VI which proved that the SHF Ground Mobile Forces Terminals, even when equipped with eight-foot parabolic dishes in a tactical environment, can make complete use of the single transponder channel. However, the system used was one with a probability of error of $10^{-5}$ and with BPSK modulation. Moreover, in a tactical environment, it is extremely difficult, if not impossible, to control the aggregate drive level to the input of the TWT. Hence, a single input which drives the TWT into

saturation is more appropriate. For a specific $P_e$, Fig 13 in Chapter IV can be used to find the required SNR at the input to both the satellite channel and the ground receiver when a single TDMA/PSK user accesses the channel.

The deviation from a single access to several non-homogeneous accesses is extremely costly. Beyond doubt, it was proved in Chapter III that these accesses will experience both suppression and intermodulation distortion. How much suppression and intermodulation distortion is experienced by each of the individual signals can be calculated from Eqs (65) and (113). A method to derive the approximate magnitude of the desired and undesired terms is also included. A specific quantity can be easily calculated if a specific case is given.

Several individuals who have published articles in journals, for example, Shaft (Ref 14), have shown that the strong signal (TDMA) should be assigned a higher carrier frequency than that of the FDMA accesses. In addition, Shaft recommends, without specifying, that the individual TDMA access should be separated by a large frequency from the FDMA signals. The separation should be large enough so that the sum and difference of the carrier frequencies fall outside the desired bandwidth of the transponder channel. The application, as described above, is shown graphically in Fig 19. However, even after the concept of Fig 19 is used, only a small fraction of the transponder channel can be used. The distortion effects outweigh any benefits derived from using

FDMA signals in the presence of a TDMA signal.

Finally, it was shown in Chapter VI, Fig 17, that each of the several non-homogeneous signals will experience at the minimum 1.05 dB of suppression. Because the n FDMA signals and the TDMA signal cannot be approximated by a Gaussian distribution, the suppression factor for each of the n weak signals approaches 6 dB. The stronger TDMA signal will experience the suppression as found by using the results available in Fig 17. The suppression of the stronger TDMA signal depends on its power to the ratio of the sum power of the n FDMA signals. But it will always be greater than 1.05 dB. As Figs 11 and 13 show, a decrease in the signal-to-noise ratio results in an increase in the probability of error.

Recommended Solution

Because technology has progressed to the point where it is now feasible to design TDMA equipment that fully utilizes the entire bandwidth and power of a single transponder channel, complete and sole use of the channel by one TDMA access is recommended. Suppression and intermodulation distortion effects are eliminated. The DSCS III transponder was designed around this concept--exclusive use of a transponder channel by several homogeneous accesses or, more appropriately, a single TDMA access.

## Bibliography


1. Abramowitz, M., et al. Handbook of Mathematical Functions (Applied Mathematical Series 55). Washington D.C.: National Bureau of Standards, 1964.

2. Blachman, Nelson M. "Detectors, Bandpass Nonlinearities, and Their Optimization: Inversion of the Chebyshev Transform," IEEE Transactions on Information Theory, IT-17: 398-404 (July 1971).

3. Davenport, W.B. Jr. "Signal-to-Noise Ratios in Bandpass Limiters," Journal of Applied Physics, 24: 720-727 (June 1973).

4. _____, and W.L. Root. An Introduction to the Theory of Random Signals and Noise. New York: McGraw-Hill Book Company, 1958.

5. Glance, B. "Power Spectra of Multi-Level Digital Phase Modulated Signals," Bell Systems Technical Journal, 50: 2857-2878 (November 1971).

6. Jain, Pravin C. "Error Probabilities in Binary Angle Modulation," IEEE Transactions on Information Theory, IT-20: 36-41 (January 1974).

7. _____, and Nelson M. Blachman. "Detection of a PSK Signal Transmitted Through a Hard-Limited Channel," IEEE Transaction on Information Theory, IT-19: 623-630 (September 1973).

8. Jones, Jay J. "Hard-Limiting of Two Signals in Random Noise," IEEE Transactions on Information Theory, IT-9: 34-42 (January 1963).

9. Lesh, James R. "Signal-to-Noise Ratios in Coherent Soft Limiters," IEEE Transactions on Communications, COM-22: 803-811 (June 1974).

10. Lindsey, William C. and Marvin K. Simon. Telecommunications Systems Engineering. Englewood Cliffs: Prentice-Hall, Inc., 1973.

11. Middleton, D. An Introduction to Statistical Communications Theory. New York: McGraw-Hill Book Company, 1960.

12. Papoulis, Athanasios. Probability of Random Variables and Stochastic Processes. New York: McGraw-Hill Book Company, 1965.

13. Shaft, Paul D. "Limiting of Several Signals and Its Effect on Communication System Performance," IEEE Transactions on Communications Technology, COM-13: 504-511 (December 1965).

14. _____. "Signals Through Nonlinearities and the Suppression of Undesired Intermodulation Terms," IEEE Transactions on Information Theory, IT-18: 657-659 (September 1972).

15. Spilker, James J. Jr. Digital Communications by Satellite. Englewood Cliffs: Prentice-Hall Inc., 1977.

16. Springett, J.C., and M.K. Simon. "An Analysis of the Phase Coherent-Incoherent Output of the Bandpass Limiter," IEEE Transactions on Communications Technology, COM-19: 42-49 (February 1971).

17. Van Trees, Harry L. Detection, Estimation, and Modulation Theory. New York: John Wiley and Sons, Inc., 1968.

18. Wozencroft, John M., and Irvin Mark Jacobs. Principles of Communications Engineering. New York: John Wiley and Sons, Inc., 1965.

## Vita

Pedro Rodriguez was born on 22 February 1945 in Grulla, Texas. He graduated from high school in Rio Grande City, Texas in 1964. He joined the Air Force on 13 January 1965, and was accepted into the Airmen Education and Commissioning Program (AECP) in May 1971. He received a Bachelor of Science in Electrical Engineering from Oklahoma State University in August 1973. From OTS, he went to Keesler AFB and attended the ground electronics communications school from which he graduated in June 1974. In June 1974, he was assigned to his first job as a commissioned officer at HQ Air Force Communications Service (AFCS) and was assigned as communications systems engineer under the directorate of satellite communications. He was transferred to AFIT in December 1976 to pursue study for the degree of Master of Science in Electrical Engineering.

Permanent Home Address: P.O. Box 178
Grulla, Texas 78548

UNCLASSIFIED

SECURITY CLASSIFICATION OF THIS PAGE (When Data Entered)

| REPORT DOCUMENTATION PAGE | | READ INSTRUCTIONS BEFORE COMPLETING FORM |
|---|---|---|
| 1. REPORT NUMBER<br>AFIT/GE/EE/78-39 | 2. GOVT ACCESSION NO. | 3. RECIPIENT'S CATALOG NUMBER |
| 4. TITLE (and Subtitle)<br>SIMULTANEOUS NON-HOMOGENEOUS MULTIPLE ACCESS TECHNIQUES | | 5. TYPE OF REPORT & PERIOD COVERED<br>MS Thesis<br>6. PERFORMING ORG. REPORT NUMBER |
| 7. AUTHOR(s)<br>Pedro Rodriguez<br>Captain USAF | | 8. CONTRACT OR GRANT NUMBER(s) |
| 9. PERFORMING ORGANIZATION NAME AND ADDRESS<br>Air Force Institute of Technology (AFIT-EN)<br>Wright-Patterson AFB, Ohio 45433 | | 10. PROGRAM ELEMENT, PROJECT, TASK AREA & WORK UNIT NUMBERS |
| 11. CONTROLLING OFFICE NAME AND ADDRESS<br>Hq AFCS (XPQS)<br>Scott AFB, Ill 62225 | | 12. REPORT DATE<br>December 1978<br>13. NUMBER OF PAGES<br>81 |
| 14. MONITORING AGENCY NAME & ADDRESS(if different from Controlling Office) | | 15. SECURITY CLASS. (of this report)<br>UNCLASSIFIED<br>15a. DECLASSIFICATION/DOWNGRADING SCHEDULE |

16. DISTRIBUTION STATEMENT (of this Report)

Approved for public release; distribution unlimited

17. DISTRIBUTION STATEMENT (of the abstract entered in Block 20, if different from Report)

18. SUPPLEMENTARY NOTES

Approved for public release; AFR 190-17

Hipps, Joseph P. Major, USAF
Director of Information 1-19-79

19. KEY WORDS (Continue on reverse side if necessary and identify by block number)

Multiple Access

20. ABSTRACT (Continue on reverse side if necessary and identify by block number)

The possibility of using simultaneous non-homogeneous multiple access techniques through a common transponder channel was investigated. Three configurations were analyzed: 1) a single time division multiple access, 2) several frequency division multiple accesses, and 3) the combined accesses of configurations 1) and 2). Each of the configurations was studied in three disjoint segments: 1) the bandwidth and shape of the power spectrum for various modulating waveforms, 2) the probability of error for

DD FORM 1 JAN 73 1473 EDITION OF 1 NOV 65 IS OBSOLETE

UNCLASSIFIED

SECURITY CLASSIFICATION OF THIS PAGE (When Data Entered)

linear PSK and non-linear PSK systems, and 3) the distortion effects that a signal experiences through a non-linearity. Each segment was studied in detail independently of the others. The comprehensive analysis accomplished on each segment, when joined into a system, allows the end-to-end channel characterization. A link calculation was accomplished for a single TDMA access, because it was found to be the optimum system based on the analysis of the segments. Also, the results obtained indicate that the benefits derived by using non-homogeneous accesses through a common transponder channel are far less than the total degradation the system experiences. A recommended alternative is provided.